Title

The targeted delivery of doxorubicin with transferrin-conjugated block copolypeptide vesicles

Journal

International Journal of Pharmaceutics, 496(2)

ISSN

0378-5173

Authors

Lee, Brian S
Yip, Allison T
Thach, Alison V
et al.

Publication Date

2015-12-01

DOI

10.1016/j.ijpharm.2015.10.028

Peer reviewed

Elsevier Editorial System(tm) for
International Journal of Pharmaceutics
Manuscript Draft

Manuscript Number: IJP-D-15-00910R1

Title: The targeted delivery of doxorubicin with transferrin-conjugated block copolypeptide vesicles

Article Type: Research Paper

Section/Category: Pharmaceutical Nanotechnology

Keywords: vesicle, block copolypeptide, drug delivery, drug release, doxorubicin, mathematical modeling

Corresponding Author: Prof. Daniel Kamei, PhD

Corresponding Author's Institution: UCLA

First Author: Brian S Lee

Order of Authors: Brian S Lee; Allison T Yip; Alison V Thach; April R Rodriguez; Timothy J Deming; Daniel Kamei, PhD

Abstract: We previously investigated the intracellular trafficking properties of our novel poly(L-glutamate)60-b-poly(L-leucine)20 (E60L20) vesicles (EL vesicles) conjugated to transferrin (Tf). In this study, we expand upon our previous work by investigating the drug encapsulation, release, and efficacy properties of our novel EL vesicles for the first time. After polyethylene glycol (PEG) was conjugated to the vesicles for steric stability, doxorubicin (DOX) was successfully encapsulated in the vesicles using a modified pH-ammonium sulfate gradient method. Tf was subsequently conjugated to the vesicles to provide active targeting to cancer cells and a mode of internalization into the cells. These Tf-conjugated, DOX-loaded, PEGylated EL (Tf-DPEL) vesicles exhibited colloidal stability and were within the allowable size range for passive and active targeting. A mathematical model was then derived to predict drug release from the Tf-DPEL vesicles by considering diffusive and convective mass transfer of DOX. Our mathematical model reasonably predicted our experimentally measured release profile with no fitted parameters, suggesting that the model could be used in the future to manipulate drug carrier properties to alter drug release profiles. Finally, an in vitro cytotoxicity assay was used to demonstrate that the Tf-DPEL vesicles exhibited enhanced drug carrier efficacy in comparison to its non-targeted counterpart.

UCLA Engineering
HENRY SAMUELI SCHOOL OF ENGINEERING AND APPLIED SCIENCE
Department of Bioengineering

DEPARTMENT OF BIOENGINEERING
HENRY SAMUELI SCHOOL OF ENGINEERING AND APPLIED SCIENCE
5121 ENGINEERING V
UCLA BOX 951600
LOS ANGELES, CA 90095-1600
(310) 206-4826
FAX (310) 794-5956

September 10, 2015

To Whom It May Concern:

The manuscript entitled:

"*The targeted delivery of doxorubicin with transferrin-conjugated block copolypeptide vesicles*"

by B.S. Lee, A.T. Yip, A.V. Thach, A.R. Rodriguez, T.J. Deming, and D.T. Kamei has been revised for consideration of publication in *International Journal of Pharmaceutics*.

We are grateful for the insightful comments from the reviewers, and have addressed all of the concerns. A detailed summary of our responses to the comments has been uploaded as the 'Lee et al Response to Reviewers' file.

Thank you very much for your time, and please do not hesitate to contact me if you have any questions.

Sincerely,

Daniel T. Kamei, Ph.D.
Professor
Department of Bioengineering

IJP AUTHOR CHECKLIST

Dear Author,

It frequently happens that on receipt of an article for publication, we find that certain elements of the manuscript, or related information, is missing. This is regrettable of course since it means there will be a delay in processing the article while we obtain the missing details.

In order to avoid such delays in the publication of your article, if accepted, could you please run through the list of items below and make sure you have completed the items.

Overall Manuscript Details

- Is this the final revised version? ■
- Are all text pages present? ■
- Are the corresponding author's postal address, telephone and fax numbers complete on the manuscript? ■
- **Have you provided the corresponding author's e-mail address?** ■
- **Manuscript type – please check one of the following:**
  - Full-length article ■
  - Review article □
  - Rapid Communication □
  - Note □
  - Letter to the Editor □
  - Other □
- **Manuscript section – paper to be published in:**
  - Pharmaceutical Nanotechnology section ■
  - Personalised Medicine section □

Manuscript elements

- Short summary/abstract enclosed? ■
- 3-6 Keywords enclosed? ■
- Complete reference list enclosed? ■
- Is the reference list in the correct journal style? ■
- Are all references cited in the text present in the reference list? ■
- Are all **original** figures cited in the text enclosed? ■
  Electronic artwork format? ---------- JPEG
- Are figure legends supplied? ■
- Are all figures numbered and orientation provided? ■
- Are any figures to be printed in colour? □
  If yes, please list which figures here:----------
- If applicable, are you prepared to pay for reproduction in colour? □
- Are all tables cited in the text supplied? ■

General

- Can you accept pdf proofs sent via e-mail? ■

***Response to Reviewers**

Authors: Brian S. Lee, Allison T. Yip, Alison V. Thach, April R. Rodriguez, Timothy J. Deming,

and Daniel T. Kamei (corresponding author)

We are grateful for the insightful comments from the reviewers, and have addressed all of their concerns. A summary of our detailed responses to their comments can be found below.

Note that the text bolded in **blue** represents text that has been added to our original document, and text bolded in **red** with the strikethrough represents text that has been removed.

Reviewer 1

1. In the Introduction (Line 55), the author claimed that the commercial DOX liposome technology has limitations, such as instability and short circulation half-life of the vesicles in the body. But this manuscript did not contain any in vitro and in vivo stability data about the Tf-DPEL, such as stability in PBS buffer or plasma. The detailed data of Tf-DPEL should be added in.

We thank the reviewer for this point regarding vesicle stability. We have removed this line from the Introduction as this was not within the scope of this paper.

Introduction (Line 52-56)

DOXIL® is currently FDA approved for treating Kaposi's sarcoma and recurrent ovarian cancer, and is under clinical trials for the treatment of multiple myeloma, breast cancer, and high-grade glioma (Imordino et al., 2006). However, there are limitations with the liposome technology, such as, liposome instability, lack of batch to batch reproducibility, and the short circulation half-life of the vesicles in the body (Barenholz, 2012).

Therefore, many researchers have been investigating new types of building blocks for developing more effective drug delivery vesicles.

Has been changed to

DOXIL® is currently FDA approved for treating Kaposi's sarcoma and recurrent ovarian cancer, and is under clinical trials for the treatment of multiple myeloma, breast cancer, and high-grade glioma (Imordino et al., 2006). ~~**However, there are limitations with the liposome technology, such as, liposome instability, lack of batch to batch reproducibility, and the short circulation half-life of the vesicles in the body (Barenholz, 2012).**~~

~~**Therefore,**~~ **In addition to liposome drug systems,** many researchers have been investigating new types of building blocks for developing more effective drug delivery vesicles.

2. In Section 3.1, the author characterized the Tf-DPEL with parameters like diameter and PDI, but without zeta potential. As we know, the zeta potential is quite important for nanoparticles, especially for stability evaluation, so this detailed data about Tf-DPEL should be included. What's more, I recommend examining the morphology of Tf-DPEL by transmission electron microscopy.

We agree with the reviewer that the zeta potential is an important value for determining the electrostatic stability of a nanoparticle system. The zeta potential was found to be -21.1 ± 2.3 mV for the extruded EL vesicles, -6.6 ± 3.5 mV upon PEGylation, and -19.5 ± 1.7 mV after conjugating Tf. These values have been included in the manuscript as well as a description about how measurements were taken.

[INSERTION after 2.8 Determining the Tf-DPEL Vesicle DOX Concentration]

2.9 Determining the Zeta Potential

In a separate set of studies, zeta potential measurements were taken using the Malvern Zetasizer. Solutions were made to contain 10% of the sample and 10% of 100 mM NaCl in filtered Rockland Ultrapure Sterile Water (i.e., deionized water). Measurements were taken after the EL vesicles were extruded, PEGylated, and conjugated with Tf.

[INSERTION after 3.1 Characterization of the Tf-DPEL Vesicles (line #416)]

Vesicle stability was further evaluated by measuring the zeta potential throughout the conjugation process. A separate set of studies was performed in order to determine the zeta potential of the EL vesicles upon extrusion, PEGylation, and Tf conjugation. The values were found to be -21.1 ± 2.3 mV for the extruded EL vesicles, -6.6 ± 3.5 mV upon PEGylation, and -19.5 ± 1.7 mV after conjugating Tf. Due to the no slip boundary condition being positioned further from the surface of charge, the decrease in the magnitude of the zeta potential was expected when the EL vesicles were coated with a layer of PEG. The zeta potential was also expected to become more negative with Tf conjugation as Tf is net negative at the pH of the buffer used during measurement. Similar to the PdI values, the resulting zeta potential values suggested that the vesicles remained stable after all conjugation procedures. Although -6.6 mV would generally represent instability, these vesicles were still stable due to the steric stabilization provided by the PEG.

The decrease in the magnitude of the zeta potential is expected when the vesicles are coated with a layer of PEG, which provides steric stability. As suggested by the DLVO theory developed by Derjaguin, Landau, Verwey, and Overbeek, the stability of a colloidal system is dependent on both attractive van der Waals forces and repulsive electrostatic interactions between particles. With respect to our vesicle construct, the effect of a PEG coating is sufficient to keep the vesicles separated by steric, excluded-volume repulsions, minimizing the effect of attractive van der

Waals forces that would cause our vesicles to aggregate.

This steric stabilization is not captured by the zeta potential, which measures the electrostatic potential at the no slip boundary. For example, let us consider a case as demonstrated by the schematic seen below, in which the no slip boundary for the EL vesicle is at $r = R$, where r is the radius, and the no slip boundary for the PEL (PEGylated EL vesicles) is at $r = a$.

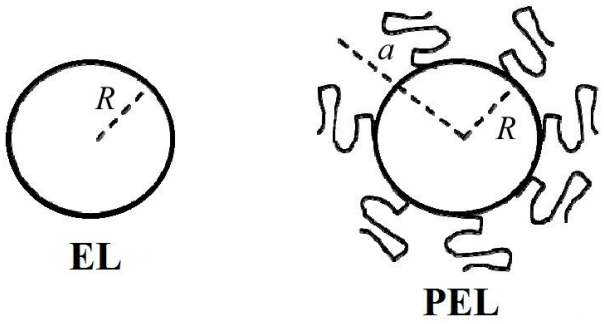

The zeta potentials would then be:

$$\zeta_{EL} = \psi_{EL}(r = R^{+}) \quad (1)$$

$$\zeta_{PEL} = \psi_{PEL}(r = a^{+}) \quad (2)$$

Where ζ_{EL} and ζ_{PEL} are the zeta potentials of the EL and PEL, respectively, and ψ_{EL} and ψ_{PEL} represent the electrostatic potentials at certain radial positions of the EL and PEL, respectively.

To derive an expression for the zeta potential of the PEL, we can first divide it into three regions similar to the figure shown below. Let us assume that although water can enter region II, salt ions do not enter this region.

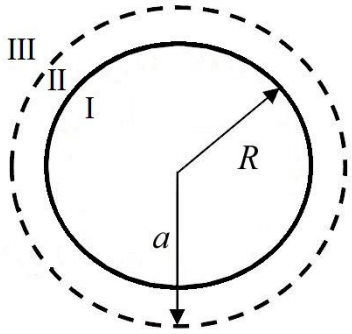

To solve for the electrostatic potential in region III (ψ_{III}), we can begin with the linearized Poisson-Boltzmann equation:

$$\nabla^2 \psi_{III}(\vec{r}) = \kappa^2 \psi_{III}(\vec{r}) \quad (3)$$

where κ^{-1} is the Debye- Hückel screening length. If we assume our vesicles to be spherically symmetric, there is no dependence on θ or ϕ, and Eq. (3) in the spherical coordinate system can be simplified to:

$$\frac{1}{r}\frac{d}{dr}\left(r^2\frac{d\psi_{III}}{dr}\right)=\kappa^2\psi_{III} \tag{4}$$

Once solved, the ordinary differential equation (ODE) represented by Eq. (4) becomes:

$$\psi_{III}=A_1\frac{\exp(-\kappa r)}{r}+A_2\frac{\exp(-\kappa r)}{r} \tag{5}$$

where A_1 and A_2 are unknown constants of integration that can be solved for with two boundary conditions. At distances very far from the PEL, we can assume that the electrostatic potential approaches zero. This boundary condition can be written as:

$$\lim_{r\to\infty}\psi_{III}\to 0 \tag{6}$$

When the first boundary condition, Eq. (6), is applied to Eq. (5), we find that $A_2=0$ and the second term drops out to yield:

$$\psi_{III}=A_1\frac{\exp(-\kappa r)}{r} \tag{7}$$

To solve for A_1, another boundary condition is required, and we can use Gauss's Law in Eq. (8) to draw a Gaussian surface just outside the PEL at $r=a^+$. Here, ε_w is the permittivity of water, ε_0 is the permittivity of free space, and q is the included charge.

$$\oint\varepsilon_w\vec{E}\cdot d\vec{S}=\frac{q}{\varepsilon_0} \tag{8}$$

Since the electric field is the negative gradient of the electrostatic potential ($\vec{E}=(-\vec{\nabla}\psi)$), we can relate the expression for electrostatic potential to the total charge enclosed by the PEL. Therefore, when Eq. (8) is applied to Eq. (7), A_1 can be solved to be equal to:

$$A_1=\frac{q\exp(\kappa a)}{4\pi\varepsilon_0\varepsilon_w(1+a\kappa)} \tag{9}$$

Therefore, by substituting Eq. (9) into Eq. (7) , Eq. (7) can be simplified as follows:

$$\psi_{III}=\frac{q}{4\pi\varepsilon_0\varepsilon_w(1+\kappa a)}\cdot\frac{\exp[-\kappa(r-a)]}{r} \tag{10}$$

Now that we have an expression for the electrostatic potential of the PEL, we can determine the zeta potential by evaluating the electrostatic potential at the no slip boundary. After combining Eqs. (2) and (10), we obtain:

$$\zeta_{PEL} = \frac{q}{4\pi\varepsilon_0\varepsilon_w(1+\kappa a)} \tag{11}$$

Likewise, it is possible to determine the zeta potential for the EL. In this case, the EL will only be divided into two regions where region I is at $r < R$ and region II is at $r > R$. Through a similar systematic analysis, we can derive the expression for the electrostatic potential of the EL vesicle to be:

$$\psi_{\text{II}} = \frac{q}{4\pi\varepsilon_0\varepsilon_w(1+\kappa R)} \cdot \frac{\exp[-\kappa(r-R)]}{r} \tag{12}$$

Combining Eqs. (1) and (12) yields the zeta potential for solely the EL:

$$\zeta_{EL} = \frac{q}{4\pi\varepsilon_0\varepsilon_w R(1+\kappa R)} \tag{13}$$

To determine the relationship between the two zeta potentials, given by Eqs. (11) and (13), we take a ratio of ζ_{EL} to ζ_{PEL} and obtain the following:

$$\text{ratio} = \left(\frac{a}{R}\right)\left(\frac{1+\kappa a}{1+\kappa R}\right) \tag{14}$$

Equation (14) provides valuable information since $a > R$, and we see that the ratio of the two zeta potentials is greater than 1. Accordingly, based on zeta potential measurements, it will appear as if the PEL is less stable since the magnitude of the electrostatic potential will be lower due to the no slip boundary being positioned further from the surface of charge. However, this is contrary to the fact since the PEG coating will provide steric stabilization, which as mentioned before, is not measured by the zeta potential.

We have also examined the morphology of our diblock copolypeptide vesicle system by transmission electron microscopy (TEM). An image of a transferrin conjugated, PEGylated, EL vesicle will be added to the manuscript as Figure 3 (seen below). This image will be uploaded separately as well.

[INSERTION after 2.9 Determining the Zeta Potential]

2.10. Transmission Electron Microscopy (TEM)

After all conjugation procedures, the morphology of the resulting vesicles was examined by TEM. 2.5 µL of the desired vesicle sample to be imaged was placed on an EMS carbon film 200 mesh grid (Electron Microscopy Sciences, Hatfield, Pennsylvania) and allowed to stand for 1 min. Filter paper was used to wick away excess sample before washing the grid with 6 µL of 2.5% (w/v) aqueous uranyl acetate (UA). After 2 s, the UA was wicked away with filter paper and another 6 µL of 2.5% (w/v) UA was immediately applied to the grid and allowed to stand for 1 min. Filter paper was then used to wick away residual liquid and the grid was left to air dry at ambient temperature for 3-5 min. Once completely dry, the grid was imaged using a FEI TF20 transmission electron microscope (FEI Company, Hillsboro, Oregon) at 200 kV.

[INSERTION after 3.1 Characterization of the Tf-DPEL Vesicles (line #416)]

In addition, we were interested in examining the morphology of the EL vesicles after PEGylation and Tf conjugation. Figure 3 shows a TEM image of the extruded EL vesicles after coating the surface with PEG and decorating the subsequent surface with Tf. The presence of unilamellar vesicles in Figure 3 suggests that the surface modifications provided by our conjugation protocol do not significantly alter or jeopardize the morphology of the original EL vesicles.

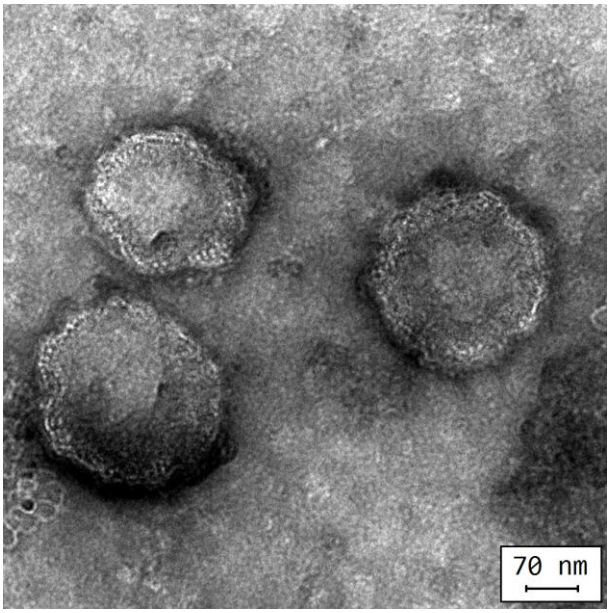

Figure 3: A transmission electron microscope (TEM) image of a uranyl acetate negatively stained EL vesicle suspension after PEGylation and Tf conjugation. Scale bar = 70 nm.

Acknowledgments (line #523)

This work was supported by the National Science Foundation DMR 1308081.

Has been changed to

This work was supported by the National Science Foundation DMR 1308081. **The authors acknowledge the help of Wong Hoi Hui and the use of instruments at the Electron Imaging Center for NanoMachines supported by NIH (1S10RR23057 to AHA) and CNSI at UCLA.**

3. In section 3.4, the author compared the in vitro cytotoxicity of Tf-DPEL with DPEL vesicles to illustrate its better targeting efficacy. I recommend adding two groups, free DOX without vesicles and DPEL vesicles with non-conjugated Tf to fully evaluate the drug delivery efficacy of Tf-DPEL. In addition, it would be better to add anti-tumor experiment *in vivo*.

We appreciate the reviewer's suggestions. With regard to the comment about *in vivo* anti-tumor studies, such studies were outside the scope of this manuscript. With regard to the additional controls for our *in vitro* cytotoxicity results, we will discuss these below.

Free doxorubicin (DOX) exhibits its cytotoxic effects by intercalating with DNA to prevent DNA biosynthesis, damaging DNA by inhibition of topoisomerase II, and generating free radicals (Gewitz *et al*., *Biochemical Pharmacology*, **57**: 727-741 (1999)). In order to act on the cell DNA, the molecule must enter the cell. Literature has shown that free DOX can enter cells by diffusion through the lipid domain of the cell membrane (Dalmark, M., Storm, H., *J. Gen. Physiol*., **78**: 359-364 (1981)). Therefore, free DOX can exert its toxic effects without active targeting. Accordingly, an *in vitro* cytotoxicity study using free DOX without vesicles would result in quick and nonspecific cell death since all the free DOX would already be in the cell media and could enter any of the cells by passive diffusion. This would not be an effective control against the Tf-DPEL vesicles since we wanted to show that the targeting effect of the Tf-DPEL vesicles, which allows the vesicles to enter and release the drug inside a specific cell, results in more effective cell death compared to DOX that is released over time by a non-targeted DPEL outside the cell. For this reason, we did not perform this *in vitro* cytotoxicity control study.

An *in vitro* cytotoxicity experiment with the DPEL vesicles with non-conjugated Tf is expected to exhibit a similar cytotoxicity as that of the DPEL vesicles alone. Previous studies have been performed with the EL vesicles to show transferrin-conjugated EL (Tf-EL) vesicles have decreased uptake into cells in the presence of excess Tf (Choe *et al*,. *Biomacromolecules* **14**: 1458-1464 (2013)). In this study, the EL vesicles were labeled with fluorescein isothiocyanate (FITC) for visualization during the intracellular trafficking studies. Tf was then conjugated to the EL vesicles. The Tf-EL vesicles were incubated with LAPC-4 and PSCA-transfected 22Rv1 cells, and the fluorescence in the cells was observed. The method of internalization was determined by using drugs that inhibit specific pathways. Additionally, the internalization of the

Tf-EL vesicles was tested in the presence of an excess of free Tf molecules. The results from this study are shown in the figure below.

In the figure below, panels (a) and (i) show the Tf-EL uptake with no inhibitor for LAPC-4 and PSCA-transfected 22Rv1 cells, respectively. The cells in these two panels displayed enhanced fluorescence in the cells, suggesting greater vesicle uptake due to the Tf targeting. Panels (d) and (l) show the cellular uptake of the Tf-EL vesicles in the presence of excess Tf for LAPC-4 and PSCA-transfected 22Rv1 cells, respectively. Both of these panels show greatly decreased fluorescence levels, demonstrating that the excess Tf is able to outcompete the Tf on the vesicles, thus preventing vesicle uptake. Additionally, there is very minimal vesicle uptake in the presence of excess Tf. This would suggest that the DPEL vesicles would also experience very minimal uptake in the presence of excess Tf. Based on this previously published study, we did not perform the cytotoxicity study with the DPEL vesicles in the presences of non-conjugated Tf since it is expected to exhibit similar cytotoxicity as DPEL vesicles alone.

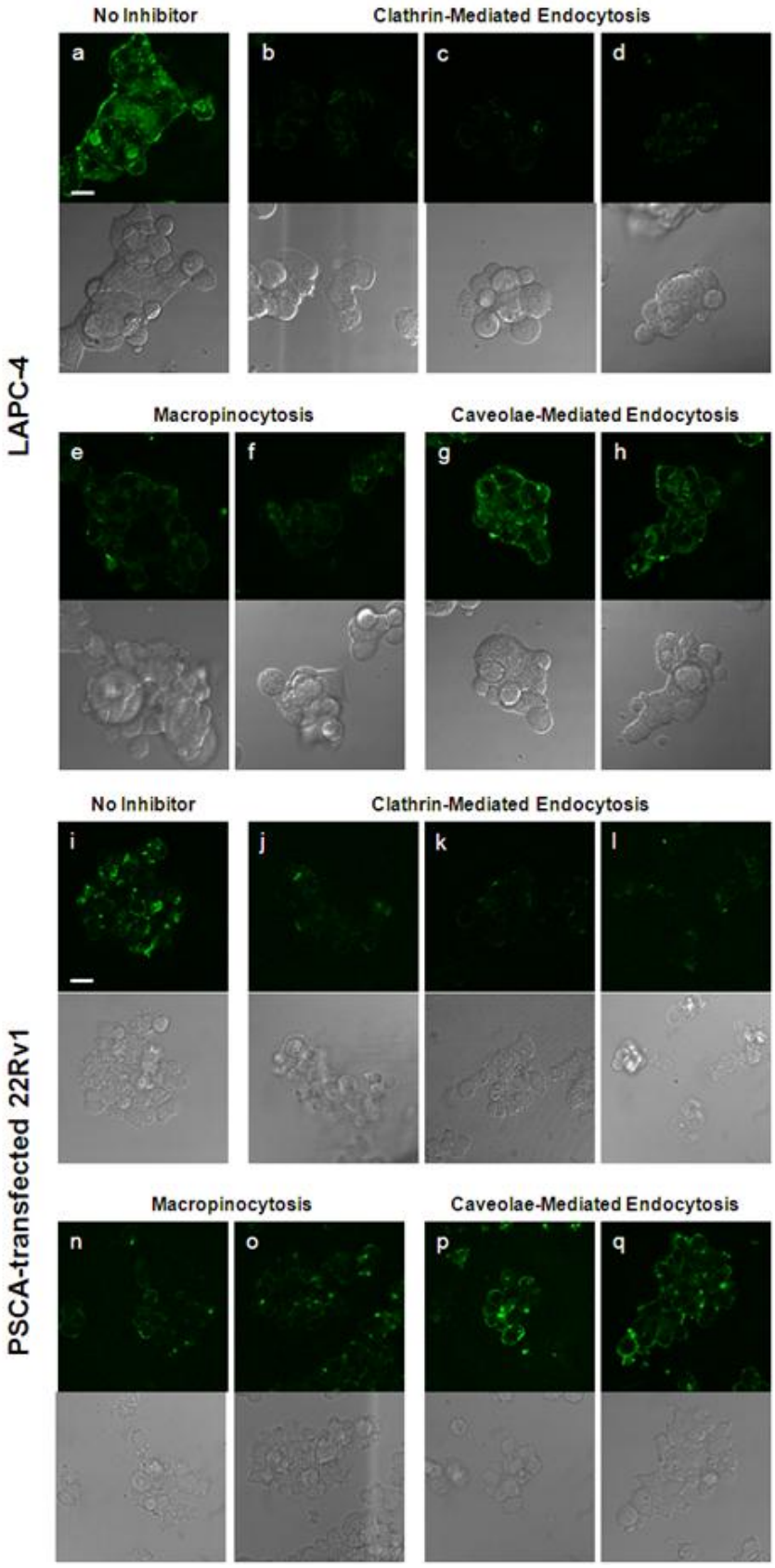
No Inhibitor
Clathrin-Mediated Endocytosis
a
b
c
d
LAPC-4
Macropinocytosis
Caveolae-Mediated Endocytosis
e
f
g
h
No Inhibitor
Clathrin-Mediated Endocytosis
i
j
k
l
PSCA-transfected 22Rv1
Macropinocytosis
Caveolae-Mediated Endocytosis
n
o
p
q

Reviewer 2

1. Summary – there is some concern around the release model validity. Only a single experiment was compared to the model and the PDI of these vesicles was ~0.2 –indicating multiple populations of vesicles. As scattering intensity is size dependent, larger particles will overshadow smaller particles – thus providing an incorrect size to input into the release model. It would be best to possibly test at least 2-3 different size vesicles and compare this release profile to the model. This information would greatly enhance the validity of the model and impact of this manuscript.

Regarding testing vesicles of different sizes to substantiate the validity of the release model, the release figure in the manuscript was an average of three release studies performed on three separate Tf-DPEL vesicle formulations. Each release study had different Tf-DPEL vesicle sizes: 128 nm, 176 nm, and 177.5 nm, although two samples coincidently had very similar sizes. We have provided the predicted release profile based on the mathematical model and their respective release study data to show that the mathematical model can account for these different vesicle sizes.

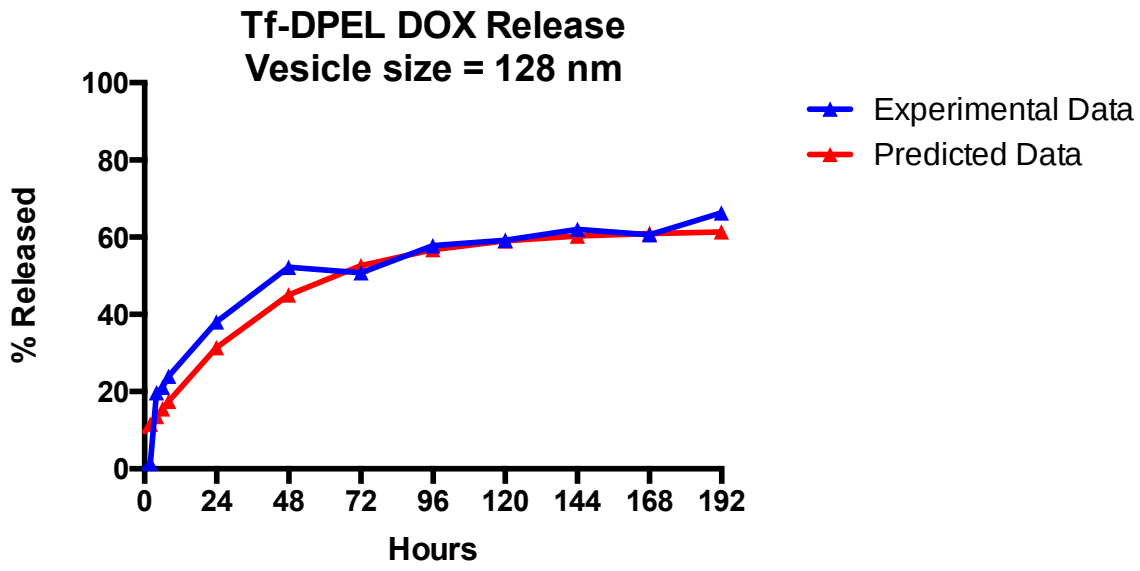

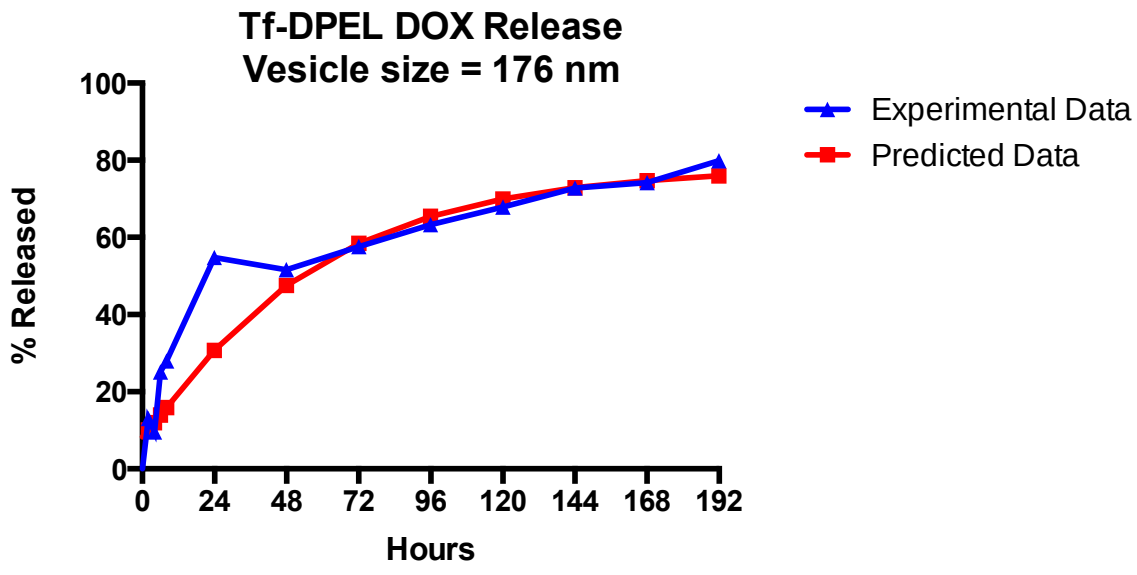

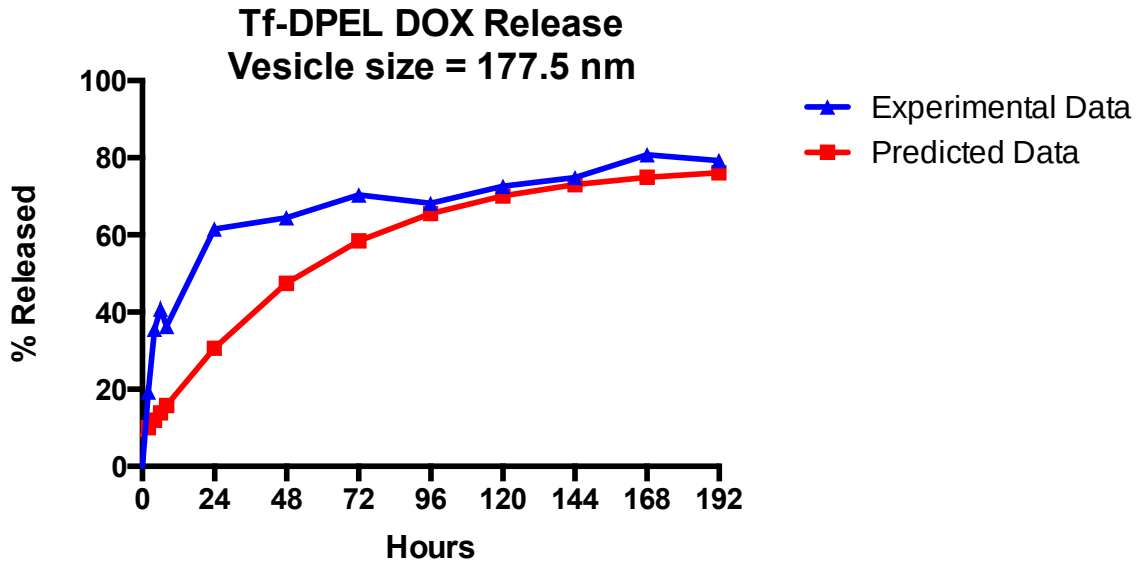

The three release profile figures above display that the mathematical model is applicable for predicting the release profile for different Tf-DPEL vesicle sizes. For the 128 nm vesicle size, the mathematical model accurately predicted the release profile trend as shown by the coinciding release profiles. For the 176 nm and 177.5 nm vesicle sizes, which had similar predicted release profiles, the actual release data exhibited a burst release in the earlier time points unaccounted for by the mathematical model, which was discussed in the manuscript. However, the mathematical model still reasonably predicted the overall trend in release data.

2. Title - Majority of the manuscript is on the processing of vesicles and a model predicting DOX release. Encapsulation was not investigated as only one drug loading of ~15 was reported. Please rephrase the title.

We thank the reviewer for this oversight on our part, and the title has been changed accordingly.

Title (line #1-2) The Encapsulation and Targeted Delivery of Doxorubicin with Transferrin-Conjugated Block Copolypeptide Vesicles *Has been changed to* The ~~**Encapsulation and**~~ Targeted Delivery of Doxorubicin with Transferrin-Conjugated Block Copolypeptide Vesicles

3. Graphical Abstract pg 2 - Low quality image – can't read text. Please modify

The image has been modified to improve the text (see below). The updated image will be uploaded separately as well.

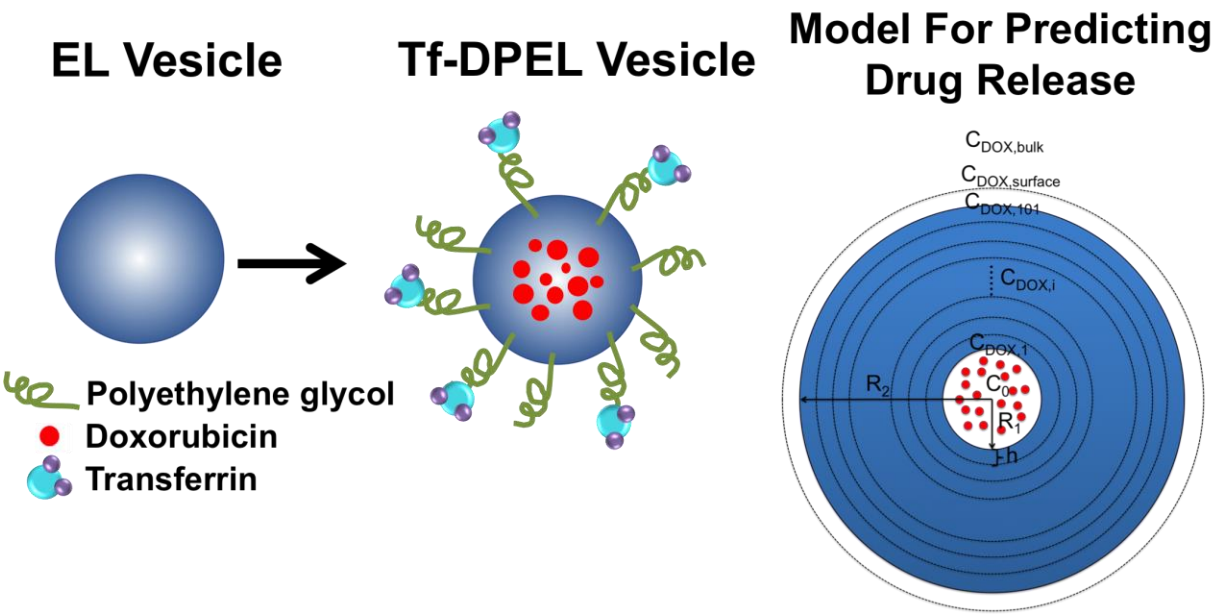

4. Line 110 - Millipore is from MA, not CA

Thank you for correcting that mistake. The text has been appropriately modified.

Materials and Methods – 2.1. Materials (line #109-110)

Spin concentrators (MWCO = 10,000 Da) were purchased from Millipore (Billerica, California).

Has been changed to

Spin concentrators (MWCO = 10,000 Da) were purchased from Millipore (Billerica, ~~**California**~~ **Massachusetts**).

5. Line 139 - Rephrase to ZEN3600

We thank the reviewer for this suggestion, and have made the appropriate change.

Materials and Methods – 2.4. Extrusion of EL Vesicles (line #138-140)

The size and polydispersity index (PdI) were measured using the Malvern Zetasizer Nano ZS model Zen 3600 (Malvern Instruments Inc., Westborough, Massachusetts).

Has been changed to

The size and polydispersity index (PdI) were measured using the Malvern Zetasizer Nano ZS model ~~**Zen**~~ **ZEN**3600 (Malvern Instruments Inc., Westborough, Massachusetts).

6. Line 174 – "The first fraction that was red was collected…" Were there multiple red fractions that also contained vesicles? Were these discarded?

Size-exclusion column chromatography was used in order to obtain the purified Tf-DPEL sample after we conjugated transferrin (Tf) to the DPEL surface. We only collected the first fraction that appeared red because we were confident that this fraction contained only the Tf-DPEL population and nothing else, as confirmed by DLS. In some cases, there were additional red fractions that also contained vesicles, but these additional fractions were discarded. We did not use these additional fractions due to our concern that the purity of the Tf-DPEL population was affected by the presence of other aggregates, such as micelles.

7. Line 176 – 184: Was a blank with Tf-PEL (no DOX) prepared and analyzed at 490nm? Also, was the standard prepared as pure DOX in buffer? It appears that not enough controls were performed to adequately determine the DOX concentration as the multiple components in the vesicles may interfere at 490nm. More controls would eliminate this concern.

In order to quantify the amount of DOX within the vesicle, the standard curve used in this manuscript was prepared from known concentrations of DOX in water. We took 20 µL of each

standard solution with known DOX concentrations and mixed it in 180 µL of DMSO for 1 h prior to measuring the absorbance at 490 nm and 700 nm to create our standard curve. This procedure was used to mimic the use of the DMSO solvent to break down the vesicle bilayer in order to determine the concentration of DOX encapsulated within the Tf-DPEL vesicles.

The aforementioned procedure was chosen because we had previously performed experiments to ensure that the additional components in the vesicles would not interfere with the absorbance readings at 490 nm and 700 nm. Shown below are two graphs with data from experiments we performed to determine the effects of the multiple components of the vesicle on absorbance.

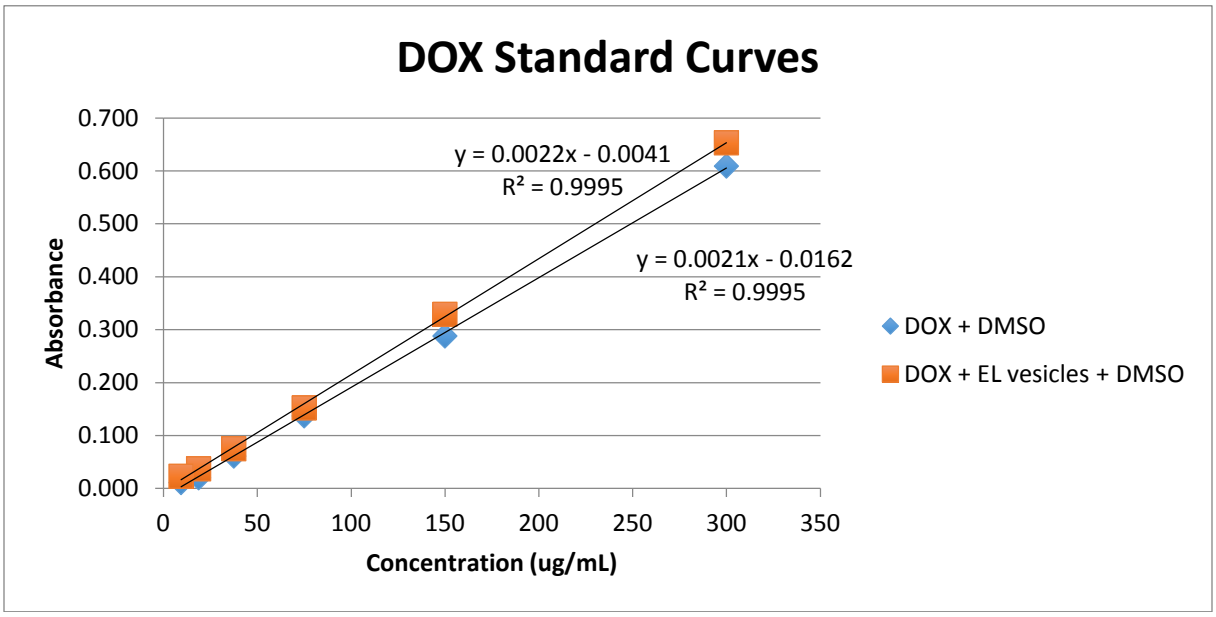

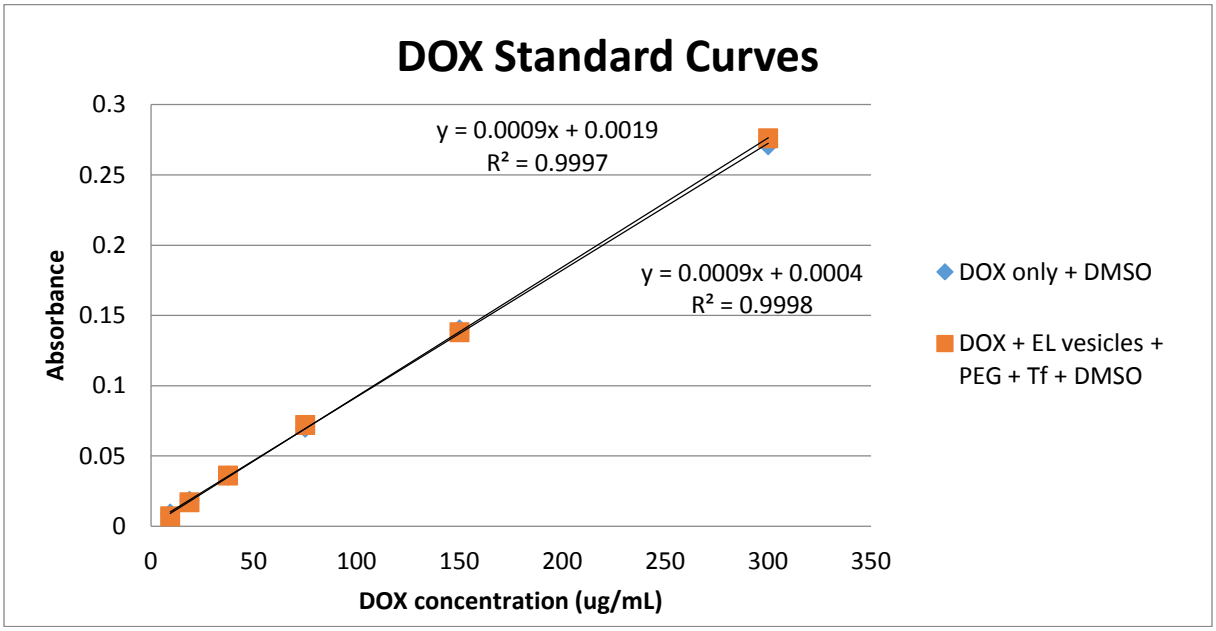

As indicated by the above data, the differences between the conditions were negligible over the range of concentrations used in the manuscript. Additionally, many of our absorbance readings were in the lower regions of the plotted data where the standard curves were very similar. We therefore concluded that the additional components of our vesicle would not interfere with the absorbance at 490 nm and 700 nm. As a result, we created our standards only with DOX in water. Note, however, that the standard curves between the two graphs are different because each curve used a different stock of DOX. Whenever we received a new DOX stock solution, we made a new standard curve.

We appreciate the reviewer's comment and have clarified our statements in the DOX quantification procedure in the manuscript text.

Materials and Methods – 2.8. Determining the Tf-DPEL Vesicle DOX Concentration (line #180-184)

The absorbance of the mixture containing Tf-DPEL vesicles and DMSO was measured at 490 nm and 700 nm using DMSO as the blank. The absorbance at 700 nm (the background absorbance) was subtracted from the absorbance at 490 nm and then compared to a standard curve with known DOX concentrations. The loading ratio was determined using the following equation:

$$Loading\ ratio\ = \frac{\mu g\ of\ DOX\ encapsulated\ in\ vesicles}{mg\ of\ initial\ polypeptide}$$

Has been changed to

The absorbance of the mixture containing Tf-DPEL vesicles and DMSO was measured at 490 nm and 700 nm using DMSO as the blank. The absorbance at 700 nm (the background absorbance) was subtracted from the absorbance at 490 nm and then compared to a standard curve with known DOX concentration. **This standard curve was created with standard solutions of DOX in water that were pipetted into DMSO to mimic the same quantification protocol as used with the vesicles. Studies were also performed to determine that the additional components of the Tf-DPEL vesicles did not interfere with the absorbance measurements at 490 nm and 700 nm (data not shown). Subsequently,** the loading ratio was determined using the following equation:

$$Loading\ ratio\ = \frac{\mu g\ of\ DOX\ encapsulated\ in\ vesicles}{mg\ of\ initial\ polypeptide}$$

8. Equation 3 - "v "- term not defined.

In Equation 3, the v term stands for the velocity in the vesicle membrane. We have included this definition in the manuscript text preceding Equation 3.

Materials and Methods – 2.11~~9~~. Mathematical Modeling of Drug Release (line #191-193)

where $C_{DOX,mem}$ is the concentration of DOX at any point in the membrane, t is time, r is the radial distance from the center of the vesicle, θ is the polar angle (taken from the z-axis), and $\emptyset$ is the azimuthal angle (on the xy-plane).

Has been changed to

where $C_{DOX,mem}$ is the concentration of DOX at any point in the membrane, t is time, **$\vec{v}$ is the velocity in the vesicle membrane,** r is the radial distance from the center of the vesicle, θ is the polar angle (taken from the z-axis), and $\emptyset$ is the azimuthal angle (on the xy-plane).

9. Methods - Please state the DLS procedure followed. What was the medium (Tris buffer?). Please state the viscosity and refractive index used. Also, is the value reported based on "Intensity" or "Z- Average"?

The DLS procedure has been added to the Materials and Methods section of the manuscript. 450 µL of each sample was measured using DLS to determine the size of the vesicles. The medium varied with each sample being analyzed. Specifically, the medium was an aqueous solution of 5 µM ammonium sulfate, 50 mM Tris buffer, and HEPES Bicarbonate (50mM HEPES and 20 mM sodium bicarbonate) for the extruded EL, PEL, and Tf-DPEL vesicles, respectively. The viscosity used was 0.8872 cP, and the dispersant refractive index used was 1.330. The values reported in Table 1 are based on the z-average values found from DLS.

Materials and Methods – 2.4. Extrusion of EL Vesicles (line #140-141)

The Bradford assay was then performed using the Coomassie Blue Reagent to quantify the final concentration of vesicles by using the post-dialyzed vesicles as the standard.

Has been changed to

The Bradford assay was then performed using the Coomassie Blue Reagent to quantify the final concentration of vesicles by using the post-dialyzed vesicles as the standard. **450 µL of the extruded EL vesicles in an aqueous solution of 5 µM ammonium sulfate were then measured using dynamic light scattering (DLS) to determine the sample size and PdI. A viscosity of 0.8872 cP and a dispersant refractive index of 1.330 were used to obtain the z-average value reported as the vesicle diameter.**

Materials and Methods – 2.5. Conjugating PEG (line #151-152)

The sample size and polydispersity index (PdI) were then measured using dynamic light scattering.

Has been changed to

The sample size and ~~**polydispersity index (**~~PdI~~**)**~~ were then measured using ~~**dynamic light scattering**~~ **a DLS protocol similar to the one used for extruded EL vesicles except the medium used for the PEL vesicles was an aqueous solution of 50 mM Tris Buffer**.

Materials and Methods – 2.7. Conjugating Transferrin (line #174-175)

The first fraction that was red was collected and verified by dynamic light scattering (DLS) to contain the desired Tf-DPEL population.

Has been changed to

The first fraction that was red was collected and verified by ~~**dynamic light scattering (**~~DLS~~**)**~~ **in an aqueous HEPES bicarbonate (50 mM HEPES and 20 mM sodium bicarbonate)** solution to contain the desired Tf-DPEL population.

10. Table 1 – Drug loading is low considered many have reported up to 99% encapsulation. Please clarify.

When Tf was conjugated to the DPEL vesicles, the DPEL vesicles were in a concentrated sample volume after spin concentrating. After conjugation, the final Tf-DPEL vesicles were purified from free, unconjugated Tf as well as other aggregates by size-exclusion column

chromatography. Once the Tf-DPEL vesicle sample was added into the column, elution buffer was added to aid in the flow. This elution buffer diluted the initially concentrated sample. Additionally, as the Tf-DPEL vesicles passed through the size-exclusion column, DOX was slowly released during this process, reducing the amount of encapsulated DOX. This was evident since a red solution was still observed in the column after collecting our Tf-DPEL vesicle fraction. Since we did not collect all the fractions, due to concerns that the other fractions would have DOX encapsulated in micelles and other aggregates, our sample contained a lower DOX concentration. These factors ultimately led to a lower drug loading.

11. Line 381 – Where is it stated that a monodispered population has a PDI of 0.3? Please cite. Monodispersed populations are normally around 0.1 or less.

We thank the reviewer for this clarification regarding monodispersity. Monodisperse populations indeed have a PdI around 0.1 or less, while a PdI less than 0.3 indicates a homogenous population with a narrow size distribution. Appropriate changes have been made to the manuscript, and the sources discussing the 0 to 0.3 PdI range have been referenced and cited in the manuscript.

Results and Discussion – 3.1. Characterization of the Tf-DPEL Vesicles (line #345-348)

By performing serial extrusion of the vesicles through 1000, 400, and 200 nm polycarbonate filters in the presence of a buffered ammonium sulfate solution, we were able to generate a monodisperse population of vesicles with a diameter of 179 nm (Table 1).

Has been changed to

By performing serial extrusion of the vesicles through 1000, 400, and 200 nm polycarbonate filters in the presence of a buffered ammonium sulfate solution, we were able to generate a ~~**monodisperse**~~ **homogeneous** population of vesicles with a diameter of 179 nm (Table 1).

Results and Discussion – 3.1. Characterization of the Tf-DPEL Vesicles (line #379-381)

Vesicle stability was assessed using the polydispersity index (PdI). The PdI values of the EL, PEL, and Tf-DPEL vesicles were 0.170, 0.198, and 0.190, respectively (Table 1). All PdI values were within the accepted range of 0 to 0.300 for a fairly monodisperse population.

Has been changed to

Vesicle stability was assessed using the polydispersity index (PdI). The PdI values of the EL, PEL, and Tf-DPEL vesicles were 0.170, 0.198, and 0.190, respectively (Table 1). All PdI values were within the range of 0 to 0.300, indicating a fairly ~~**monodisperse**~~ **homogeneous** population **(Badran et al., 2012), (Ibrahim et al., 2014)**.

12. Line 411-422 – The description of how R1 and R2 are calculated measured should be placed in the Methods section, not in the Results. R1 and R2 were stated previously but not explained, which may lead to confusion.

We thank the reviewer for this oversight on our part. This description has been moved to the Methods section.

Results and Discussion – 3.3. Predicted and Measured In Vitro Drug Release Profiles for the Tf-DPEL Vesicles (line #405-425)

To accurately predict DOX release from the Tf-DPEL vesicles, parameters such as the vesicle core radius R_1, the total radius R_2, the partition coefficient of DOX K, the diffusion coefficient of DOX in the vesicle bilayer D_{DOX}, and the convective mass transfer coefficient for DOX in water k_c were determined based on previously measured data or values reported in the literature. First, R_2 was estimated by the DLS measurement presented in Table 1. The Tf-DPEL vesicle diameter was approximately 160 nm, so the radius R_2 was set as 80 nm. The inner radius of the vesicle core, R_1, was calculated by subtracting the bilayer thickness from the R_2 value. We have previously reported a method for calculating the EL vesicle bilayer thickness (Choe et al., 2013). Specifically, when the $E_{60}L_{20}$ polypeptides self-assemble into vesicles, we believe that the polypeptides align such that the hydrophobic membrane has a thickness equal to the length of one hydrophobic L_{20} segment. Since the L_{20} segments form alpha-helices, which typically have 3.6 residues per turn and 5.4 Å per turn, the hydrophobic membrane thickness was calculated as 20 residues multiplied by 5.4 Å per 3.6 residues, equaling 3 nm. The hydrophilic E_{60} segments of adjacent polypeptides face in opposite directions, either inwards or outwards, to create the hydrophilic membranes. The average distance of 3.4 Å per glutamate residue was used to calculate the thickness of the E_{60} segments, which were approximated as random coils (Choe et al., 2013). Since two hydrophilic membranes are created by the inward and outward facing E_{60} segments, the collective hydrophilic membrane thickness was estimated to be 40.8 nm. The entire vesicle membrane was determined by adding the thickness of the hydrophobic membrane to the hydrophilic membranes, resulting in a value of 40.8 + 3 = 43.8 nm. The inner radius of R_1 was then calculated as 80 - 43.8 = 36.2 nm.

The DOX diffusion coefficient in the Tf-DPEL vesicle bilayer was selected based on values reported for a similar vesicle system.

Has been changed to

To accurately predict DOX release from the Tf-DPEL vesicles, parameters such as the vesicle core radius R_1, the total radius R_2, the partition coefficient of DOX K, the diffusion coefficient of DOX in the vesicle bilayer D_{DOX}, and the convective mass transfer coefficient for DOX in water k_c were determined based on previously measured data or values reported in the literature. **~~First, R_2 was estimated by the DLS measurement presented in Table 1. The Tf-DPEL vesicle diameter was approximately 160 nm, so the radius R_2 was set as 80 nm. The inner radius of the vesicle core, R_1, was calculated by~~**

~~subtracting the bilayer thickness from the R_2 value. We have previously reported a method for calculating the EL vesicle bilayer thickness (Choe et al., 2013). Specifically, when the $E_{60}L_{20}$ polypeptides self-assemble into vesicles, we believe that the polypeptides align such that the hydrophobic membrane has a thickness equal to the length of one hydrophobic L_{20} segment. Since the L_{20} segments form alpha-helices, which typically have 3.6 residues per turn and 5.4 Å per turn, the hydrophobic membrane thickness was calculated as 20 residues multiplied by 5.4 Å per 3.6 residues, equaling 3 nm. The hydrophilic E_{60} segments of adjacent polypeptides face in opposite directions, either inwards or outwards, to create the hydrophilic membranes. The average distance of 3.4 Å per glutamate residue was used to calculate the thickness of the E_{60} segments, which were approximated as random coils (Choe et al., 2013). Since two hydrophilic membranes are created by the inward and outward facing E_{60} segments, the collective hydrophilic membrane thickness was estimated to be 40.8 nm. The entire vesicle membrane was determined by adding the thickness of the hydrophobic membrane to the hydrophilic membranes, resulting in a value of 40.8 + 3 = 43.8 nm. The inner radius of R_1 was then calculated as 80 – 43.8 = 36.2 nm.~~

R_1 and R_2 were determined as described in section 2.9.

Mathematical Modeling of Drug Release. The DOX diffusion coefficient in the Tf-DPEL vesicle bilayer was selected based on values reported for a similar vesicle system.

Materials and Methods – 2.9. Mathematical Modeling of Drug Release (line #208-211)

For the method of lines, the vesicle bilayer was first divided into a finite number of nodes as shown in Figure 1. The Tf-DPEL vesicle had an aqueous core radius of R_1 and a total radius of R_2. Since the accuracy of the numerical solution increases with the number of nodes, we divided the Tf-DPEL vesicle membrane into 101 nodes.

Has been changed to

For the method of lines, the vesicle bilayer was first divided into a finite number of nodes as shown in Figure 1. The Tf-DPEL vesicle had an aqueous core radius of R_1 and a total radius of R_2. **The values of R_1 and R_2 used in the mathematical model were determined by the following method. R_2 was estimated by DLS measurements. The inner radius of the vesicle core, R_1, was calculated by subtracting the bilayer thickness from the R_2 value. We have previously reported a method for calculating the EL vesicle bilayer thickness (Choe et al., 2013). Specifically, when the $E_{60}L_{20}$ polypeptides self-assemble into vesicles, we believe that the polypeptides align such that the hydrophobic membrane has a thickness equal to the length of one hydrophobic L_{20} segment. Since the L_{20} segments form alpha-helices, which typically have 3.6 residues per turn and 5.4 Å per turn, the hydrophobic membrane thickness was calculated as 20 residues multiplied by 5.4 Å per 3.6 residues, equaling 3 nm. The hydrophilic E_{60} segments of adjacent polypeptides face in opposite directions, either inwards or outwards, to create the hydrophilic membranes. The average distance of 3.4 Å per glutamate residue was used to calculate the thickness of the E_{60} segments, which were approximated as random coils (Choe et al., 2013). Since two hydrophilic membranes are created by the inward and outward facing E_{60} segments, the collective hydrophilic membrane thickness was estimated to be 40.8 nm. The entire vesicle membrane was determined by adding the thickness of the hydrophobic membrane to the hydrophilic membranes, resulting in a value of 40.8 + 3 = 43.8 nm. The Tf-DPEL vesicle diameter was approximately 160 nm, so the radius R_2 was set as 80 nm. The inner radius of R_1 was then calculated as 80 - 43.8 = 36.2 nm.**

Since the accuracy of the numerical solution increases with the number of nodes, we divided the Tf-DPEL vesicle membrane into 101 nodes.

*Graphical Abstract (for review)

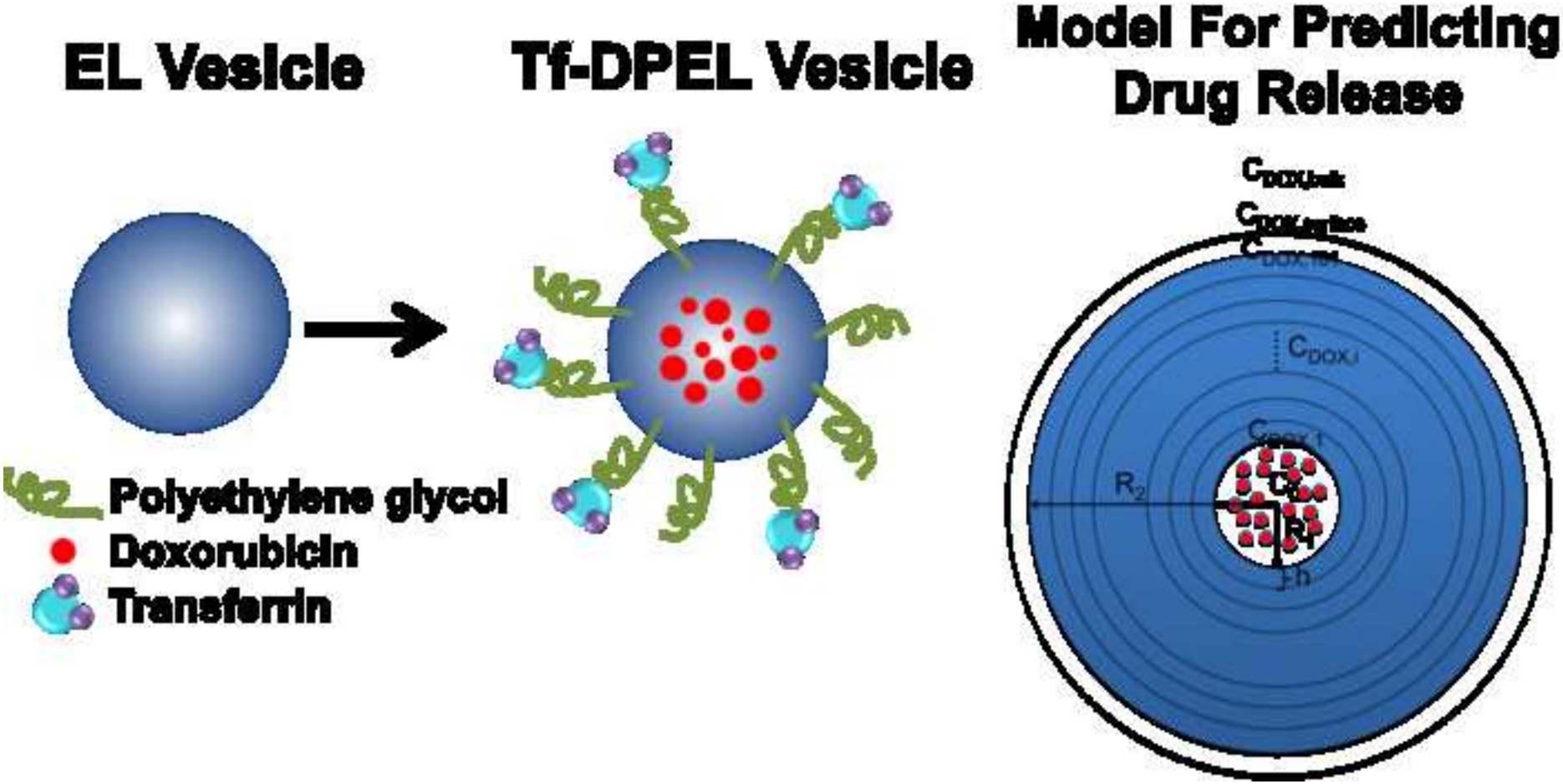

The Targeted Delivery of Doxorubicin with Transferrin-Conjugated Block Copolypeptide Vesicles

Brian S. Lee, Allison T. Yip, Alison V. Thach, April R. Rodriguez, Timothy J. Deming, and Daniel T. Kamei*

Department of Bioengineering, University of California, Los Angeles, 420 Westwood Plaza, 5121 Engineering V, Los Angeles, CA 90095

*Corresponding author: 420 Westwood Plaza, 5121J Engineering V, P.O. Box 951600, University of California, Los Angeles, CA 90095-1600, Phone: 310-206-4826, Email: kamei@seas.ucla.edu

Keywords: vesicle, block copolypeptide, drug delivery, drug release, doxorubicin, mathematical modeling

Chemical compounds studied in this article

N-hydroxysuccinimide (PubChem CID: 80170); 1-Ethyl-3-(3-dimethylaminopropyl)carbodiimide (PubChem CID: 15908); Tetrahydrofuran (PubChem CID: 8028); Ammonium Sulfate (PubChem CID: 6097028); Dimethyl Sulfoxide (PubChem CID: 679)

Abbreviations[1]

$E_{60}L_{20}$: poly(L-glutamate)$_{60}$-*b*-poly(L-leucine)$_{20}$ block copolypeptide

EL vesicles: self-assembled vesicular structures from $E_{60}L_{20}$ block copolypeptides

Tf-DPEL vesicles: transferrin-conjugated, DOX-loaded, PEGylated EL vesicles

[1] $E_{60}L_{20}$: poly(L-glutamate)$_{60}$-*b*-poly(L-leucine)$_{20}$ block copolypeptide
EL vesicles: self-assembled vesicular structures from $E_{60}L_{20}$ block copolypeptides
Tf-DPEL vesicles: transferrin-conjugated, DOX-loaded, PEGylated EL vesicles

Abstract

We previously investigated the intracellular trafficking properties of our novel poly(L-glutamate)$_{60}$-*b*-poly(L-leucine)$_{20}$ ($E_{60}L_{20}$) vesicles (EL vesicles) conjugated to transferrin (Tf). In this study, we expand upon our previous work by investigating the drug encapsulation, release, and efficacy properties of our novel EL vesicles for the first time. After polyethylene glycol (PEG) was conjugated to the vesicles for steric stability, doxorubicin (DOX) was successfully encapsulated in the vesicles using a modified pH-ammonium sulfate gradient method. Tf was subsequently conjugated to the vesicles to provide active targeting to cancer cells and a mode of internalization into the cells. These Tf-conjugated, DOX-loaded, PEGylated EL (Tf-DPEL) vesicles exhibited colloidal stability and were within the allowable size range for passive and active targeting. A mathematical model was then derived to predict drug release from the Tf-DPEL vesicles by considering diffusive and convective mass transfer of DOX. Our mathematical model reasonably predicted our experimentally measured release profile with no fitted parameters, suggesting that the model could be used in the future to manipulate drug carrier properties to alter drug release profiles. Finally, an *in vitro* cytotoxicity assay was used to demonstrate that the Tf-DPEL vesicles exhibited enhanced drug carrier efficacy in comparison to its non-targeted counterpart.

1. Introduction

Doxorubicin (DOX) is one of the most widely used small molecule drugs for the treatment of several cancers, such as breast and lung cancer (Keizer et al., 1990). However, the major limitation of the naked delivery of DOX is its nonspecificity, often resulting in undesirable toxicity to healthy organs and tissues (Imordino et al., 2006). Therefore, research has been performed in hopes of targeting the delivery of drugs towards only cancer cells by encapsulating the drug within nano-sized particles. Nano-sized drug delivery vehicles are advantageous since they can protect the drug from degradation during its circulation in the body, release the drug in a controlled manner, and provide passive targeting to the tumor tissue through the enhanced permeability and retention (EPR) effect (Greish, 2010), (Sahoo et al., 2008).

Liposomes have shown great promise as nano-sized drug delivery vehicles. One of the most well-known liposome drug systems in the market is DOXIL®, which is a formulation of doxorubicin encapsulated within PEGylated liposomes. DOXIL® is currently FDA approved for treating Kaposi's sarcoma and recurrent ovarian cancer, and is under clinical trials for the treatment of multiple myeloma, breast cancer, and high-grade glioma (Imordino et al., 2006).

In addition to liposome drug systems, many researchers have been investigating new types of building blocks for developing more effective drug delivery vesicles. An emerging class of drug delivery vehicles is the block copolypeptide vesicle since it has properties that makes it promising as an effective carrier for therapeutics. The advantages of block copolypeptides include synthetic control of chain lengths, incorporation of secondary structure, ability to be functionalized, and potential to be biocompatible (Carlsen and Lecommandoux, 2009). Our group previously investigated a novel block copolypeptide vesicle construct, the poly(L-

glutamate)$_{60}$-*b*-poly(L-leucine)$_{20}$ ($E_{60}L_{20}$). These polypeptides self-assembled into vesicles that could be controlled in size, encapsulate hydrophilic molecules, and exhibit very low cytotoxicity towards cells (Choe et al., 2013). However, the main limitation of the $E_{60}L_{20}$ vesicles (EL vesicles) as a potential drug carrier was their inability to efficiently enter cancer cells due to the electrostatic repulsions between the negatively-charged surface and the net negatively-charged cell membrane, thus preventing interactions for cellular uptake. To overcome this limitation, transferrin (Tf) was previously conjugated onto the surfaces of the EL vesicles as Tf is a well-known targeting ligand for cancer and its intracellular trafficking properties have also been well studied (Aisen and Listowsky, 1980), (Karin and Mintz, 1981), (Mayle et al., 2012). Fluorescence and endocytosis inhibitor studies demonstrated that the Tf-EL vesicles exhibited enhanced cellular uptake into cancer cells, primarily through clathrin-mediated endocytosis (Choe et al., 2013). Since the Tf-EL vesicles were able to effectively enter cancer cells, it was hypothesized that this would translate into enhanced therapeutic efficacy if small molecule drugs were encapsulated within the EL vesicles since many chemotherapeutics, such as DOX, have intracellular targets (Tacar et al., 2012).

This study is the first investigation of the drug delivery capabilities of the EL vesicles. After conjugating polyethylene glycol (PEG) to the EL vesicles to form PEGylated EL vesicles, DOX was successfully encapsulated into the vesicles using a modified pH-ammonium sulfate gradient. Tf was then conjugated to the vesicles to create a targeted drug delivery system: the Tf-conjugated, DOX-loaded, PEGylated EL (Tf-DPEL) vesicle. The size and stability of the Tf-DPEL vesicles were monitored using dynamic light scattering, and the drug loading ratio was evaluated after the formation of the Tf-DPEL vesicles. Zeta potential measurements were additionally taken to evaluate the stability of the vesicles throughout the conjugation process and

the resulting vesicles were imaged using transmission electron microscopy (TEM). Moreover, a mathematical model was derived to predict the drug release properties of the Tf-DPEL vesicles. In our mathematical model, we considered the transient diffusion of DOX across the vesicle bilayer as described by the Conservation of Species equation. Mass balance and convective mass transfer equations modeled drug release from the vesicle surface to the bulk solution. The resulting system of differential equations was solved numerically using finite difference equations and the method of lines. *In vitro* release studies were performed to compare with the drug release properties predicted by the mathematical model. *In vitro* cytotoxicity studies also demonstrated that the Tf-DPEL vesicles exhibited an improved therapeutic effect compared to the non-targeted DPEL vesicles.

2. Materials and Methods

2.1. Materials

The Bradford reagent was obtained from Bio-Rad (Hercules, California). Dialysis bags (MWCO = 8,000 Da) were obtained from Spectrum Laboratories (Rancho Dominguez, California). The 1000, 400, and 200 nm polycarbonate membranes were purchased from Whatman Nuclepore (Florham Park, New Jersey). The Avanti Mini-Extruder was purchased from Avanti Polar Lipids Inc. (Alabaster, Alabama). Zeba desalt spin columns (MWCO = 8,000 Da), N-hydroxysuccinimide (NHS), and 1-ethyl-3-(3-dimethylaminopropyl) carbodiimide (EDC) were obtained from Pierce (Rockford, Illinois). The methoxy-poly(ethylene glycol)$_{5000}$-amine (mPEG) and orthopyridyl disulfide-poly(ethylene glycol)$_{5000}$-amine (biPEG) molecules that were conjugated onto the vesicles were purchased from Nanocs (New York, New York). Both of these molecules have 5000 MW PEG, where mPEG is amine functionalized on one end, while biPEG is amine functionalized on one end and functionalized with an orthopyridyl disulfide (OPSS)

group on the other end. Spin concentrators (MWCO = 10,000 Da) were purchased from Millipore (Billerica, Massachussetts). UltraPure Sterile Water was purchased from Rockland Immunochemicals (Limerick, Pennsylvania). The prostate cancer cell line PC3 was obtained from the American Type Culture Collection (Manassas, Virginia). Roswell Park Memorial Institute (RPMI) 1640 medium, penicillin-streptomycin (P/S), sodium pyruvate (NaPyr), phosphate-buffered saline (PBS), and 0.25% trypsin with ethylenediaminetetraacetic acid **(**EDTA) were purchased from Invitrogen (Carlsbad, California). Fetal bovine serum (FBS) was obtained from Hyclone (Waltham, Massachusetts). The CellTiter 96® AQueous Non-radioactive Cell Proliferation Assay (MTS assay) was purchased from Promega (Madison, Wisconsin). All other reagents, such as apo-transferrin (apo-Tf), 4-(2-hydroxyethyl)-1-piperazineethanesulfonic acid (HEPES), and Sepharose CL-4B cross linked beads, were purchased from Sigma-Aldrich (St. Louis, Missouri) unless otherwise noted.

2.2. Synthesis of the $E_{60}L_{20}$ Block Copolypeptide

The $E_{60}L_{20}$ block copolypeptide was synthesized using the transition metal-mediated α-amino acid *N*-carboxyanhydride (NCA) polymerization technique, as previously described (Deming, 1997), (Holowka et al., 2005).

2.3. Processing the EL Vesicles

A solution of 0.5% w/v polypeptide in tetrahydrofuran (THF) was first prepared. This solution was sonicated for 30 min, followed by a 30 min interval of inactivity, and then another 30 min of sonication to ensure dissolution of the polypeptide. Subsequently, filtered water was added dropwise to the solution while vortexing such that the final suspension was a 2:1 volume ratio of THF to water. This resulted in a vesicle concentration of 0.333% w/v. In order to remove the remaining THF, the resulting suspension was dialyzed (MWCO = 8,000 Da) against filtered

water overnight with water bath changes every hour for the first 3 h. After dialysis, the final EL vesicle concentration was diluted to 0.2% w/v with filtered water.

2.4. Extrusion of EL Vesicles

To prepare the processed vesicles for subsequent drug loading procedures, the appropriate amount of a 50 μM ammonium sulfate solution was added such that the final suspension had an ammonium sulfate concentration of 5 μM. The vesicles were then serially extruded through 1000, 400, and 200 nm Whatman Nuclepore polycarbonate membranes using the Avanti Mini-Extruder. The size and polydispersity index (PdI) were measured using the Malvern Zetasizer Nano ZS model ZEN3600 (Malvern Instruments Inc., Westborough, Massachusetts). The Bradford assay was then performed using the Coomassie Blue Reagent to quantify the final concentration of vesicles by using the post-dialyzed vesicles as the standard. 450 μL of the extruded EL vesicles in an aqueous solution of 5 μM ammonium sulfate were then measured using dynamic light scattering (DLS) to determine the sample size and PdI. A viscosity of 0.8872 cP and a dispersant refractive index of 1.330 were used to obtain the z-average value reported as the vesicle diameter.

2.5. Conjugating PEG

PEG was conjugated onto the vesicles using EDC/NHS chemistry to activate the carboxylate groups on the EL vesicle surfaces. EDC and NHS, both at a 25,000-fold molar excess relative to vesicles, were added to the vesicle suspension, and the mixture was incubated for 25 min. A 0.5 M phosphate buffer (PB) solution was then added to raise the pH of the suspension to 7.0 and quench the reaction. Subsequently, a solution containing methoxy-poly(ethylene glycol)$_{5000}$-amine (mPEG) and orthopyridyl disulfide-poly(ethylene glycol)$_{5000}$-amine (biPEG), both at 12,500-fold molar excess relative to vesicle, was added. This mixture

was incubated for 2 h. The sample was purified using a spin concentration filter (MWCO = 10,000 Da) and suspended in 500 µL of Tris buffer. The sample size and PdI were then measured using a DLS protocol similar to the one used for extruded EL vesicles except the medium used for the PEL vesicles was an aqueous solution of 50 mM Tris Buffer.

2.6. Encapsulating Doxorubicin

DOX in filtered Ultrapure water and vesicles in Tris buffer were separately heated in a water bath at 65˚C for 2 min. The DOX solution was then added to the suspension of PEGylated vesicles in 50 mM Tris buffer at a 4:10 mass ratio of DOX to EL vesicles. This suspension was then placed in a 65˚C water bath for 1 h, followed by purification of free DOX from the DOX-loaded vesicles using a spin concentrator (MWCO = 10,000 Da).

2.7. Conjugating Transferrin

Prior to conjugating Tf, apo-Tf was iron loaded to generate holo-Tf as described in our previous study (Choe et al., 2013). Briefly, 20 µL of the iron chelating agent nitrilotriacetate (NTA) was mixed with 10 µL of 250 mM iron (III) chloride. A 1.0% w/v solution of apo-Tf in a 50 mM HEPES buffer containing 20 mM sodium bicarbonate was also prepared. The chelated iron was then added to the apo-Tf solution and allowed to iron load overnight at room temperature. The following day, holo-Tf (iron-loaded Tf) was purified from the free iron using a Zeba desalt spin column and then thiolated for 1 h using Traut's reagent. Afterward, the thiolated Tf was purified with a Zeba desalt spin column. A 10,000:1 molar ratio of thiolated Tf:vesicle was then added to the DOX loaded and PEGylated, EL (DPEL) vesicle and allowed to react overnight with constant mixing. In order to purify free Tf from the Tf-DPEL vesicles, size-exclusion chromatography was performed. A column was packed with Sepharose CL-4B beads and rinsed with 12 mL of the HEPES elution buffer. This column was then stored in a 4˚C

refrigerator until use. After the Tf conjugation, the concentrated sample was added into the column. Fractions were taken every two min while running more of the HEPES bicarbonate elution buffer through the column. The first fraction that was red was collected and verified by DLS in an aqueous HEPES bicarbonate (50 mM HEPES and 20 mM sodium bicarbonate) solution to contain the desired Tf-DPEL population.

2.8. Determining the Tf-DPEL Vesicle DOX Concentration

Following purification, the concentration of DOX within the Tf-DPEL vesicle population was determined using a Beckman Coulter UV-visible Spectrophotometer (Beckman Coulter, Brea, California). For these measurements, 20 µL of the Tf-DPEL vesicle sample were dissolved in 180 µL of DMSO for 1 h. The absorbance of the mixture containing Tf-DPEL vesicles and DMSO was measured at 490 nm and 700 nm using DMSO as the blank. The absorbance at 700 nm (the background absorbance) was subtracted from the absorbance at 490 nm and then compared to a standard curve with known DOX concentrations. This standard curve was created with standard solutions of DOX in water that were pipetted into DMSO to mimic the same quantification protocol as used with the vesicles. Studies were also performed to determine that the additional components of the Tf-DPEL vesicles did not interfere with the absorbance measurements at 490 nm and 700 nm (data not shown). Subsequently, the loading ratio was determined using the following equation:

$$Loading\ ratio\ = \frac{\mu g\ of\ DOX\ encapsulated\ in\ vesicles}{mg\ of\ initial\ polypeptide} \quad (1)$$

2.9. Determining the Zeta Potential

In a separate set of studies, zeta potential measurements were taken using the Malvern Zetasizer. Solutions were made to contain 10% of the sample and 10% of 100mM NaCl in

filtered Rockland Ultrapure Sterile Water (i.e., deionized water). Measurements were taken after the EL vesicles were extruded, PEGylated, and conjugated with Tf.

2.10. Transmission Electron Microscopy (TEM)

After all conjugation procedures, the morphology of the resulting vesicles was examined by TEM. 2.5 µL of the desired vesicle sample to be imaged was placed on an EMS carbon film 300 mesh grid (Electron Microscopy Sciences, Hatfield, Pennsylvania) and allowed to stand for 1 min. Filter paper was used to wick away excess sample before washing the grid with 6 µL of 2.5% (w/v) aqueous uranyl acetate (UA). After 2 s, the UA was wicked away with filter paper and another 6 µL of 2.5% (w/v) UA was immediately applied to the grid and allowed to stand for 1 min. Filter paper was then used to wick away residual liquid and the grid was left to air dry at ambient temperature for 3-5 min. Once completely dry, the grid was imaged using a FEI TF20 transmission electron microscope (FEI Company, Hillsboro, Oregon) at 200 kV.

2.11. Mathematical Modeling of Drug Release

We developed a mathematical model to predict DOX release from the Tf-DPEL vesicles. Our model considered the transient diffusion of DOX across the vesicle bilayer and convective mass transfer of DOX from the vesicle surface to the bulk solution, as well as mole balance equations. We began with the Conservation of Species equation, which describes the accumulation of DOX in the vesicle membrane due to convection, diffusion, and any reactions:

$$\frac{\partial C_{DOX,mem}}{\partial t} + \vec{v} \cdot \vec{\nabla} C_{DOX,mem} =$$

$$D_{DOX}\left[\frac{1}{r^2}\frac{\partial}{\partial r}\left(r^2\frac{\partial C_{DOX,mem}}{\partial r}\right) + \frac{1}{r^2 sin\theta}\frac{\partial}{\partial \theta}\left(sin\theta\frac{\partial C_{DOX,mem}}{\partial \theta}\right) + \frac{1}{r^2 sin^2 \emptyset}\frac{\partial^2 C_{DOX,mem}}{\partial \emptyset^2}\right] + \quad (2)$$

$$R_{DOX,mem}$$

where $C_{DOX,mem}$ is the concentration of DOX at any point in the membrane, t is time, $\vec{v}$ is the velocity in the vesicle membrane, r is the radial distance from the center of the vesicle, θ is the polar angle (taken from the z-axis), and $\emptyset$ is the azimuthal angle (on the xy-plane). D_{DOX} is the diffusion coefficient of DOX in the membrane, which is a physical parameter that describes the mobility of DOX in the Tf-DPEL vesicle membrane. $R_{DOX,mem}$ is a reaction term that describes the rate of synthesis or degradation of DOX in the membrane. Although there is stirring during the *in vitro* release experiment, it is a commonly used approximation to assume that the solution in the vesicle membrane is stagnant, and therefore,

$$\vec{v} = 0 \tag{3}$$

Additionally, since the vesicle is spherical and the drug concentration is expected to be spherically symmetric, there should be no dependence of drug concentration on the angular coordinates:

$$\frac{\partial C_{DOX,mem}}{\partial \theta} = \frac{\partial C_{DOX,mem}}{\partial \emptyset} = 0 \tag{4}$$

Since there is no reaction involving DOX occurring anywhere in the vesicle membrane,

$$R_{DOX,mem} = 0 \tag{5}$$

Combining Eqs. (2) - (5) yields:

$$\frac{\partial C_{DOX,mem}}{\partial t} = D_{DOX}\left(\frac{\partial^2 C_{DOX,mem}}{\partial r^2} + \frac{2}{r}\frac{\partial C_{DOX,mem}}{\partial r}\right) \tag{6}$$

To solve the partial differential equation (PDE) given by Eq. (6), numerical methods were used. Specifically, we employed finite difference equations and the method of lines to numerically

solve for the DOX concentration profile. In this method, the PDE is changed to a system of ordinary differential equations (ODEs), which can then be solved in MATLAB.

For the method of lines, the vesicle bilayer was first divided into a finite number of nodes as shown in Figure 1. The Tf-DPEL vesicle had an aqueous core radius of R_1 and a total radius of R_2. The values of R_1 and R_2 used in the mathematical model were determined by the following method. R_2 was estimated by DLS measurements. The inner radius of the vesicle core, R_1, was calculated by subtracting the bilayer thickness from the R_2 value. We have previously reported a method for calculating the EL vesicle bilayer thickness (Choe et al., 2013). Specifically, when the $E_{60}L_{20}$ polypeptides self-assemble into vesicles, we believe that the polypeptides align such that the hydrophobic membrane has a thickness equal to the length of one hydrophobic L_{20} segment. Since the L_{20} segments form alpha-helices, which typically have 3.6 residues per turn and 5.4 Å per turn, the hydrophobic membrane thickness was calculated as 20 residues multiplied by 5.4 Å per 3.6 residues, equaling 3 nm. The hydrophilic E_{60} segments of adjacent polypeptides face in opposite directions, either inwards or outwards, to create the hydrophilic membranes. The average distance of 3.4 Å per glutamate residue was used to calculate the thickness of the E_{60} segments, which were approximated as random coils (Choe et al., 2013). Since two hydrophilic membranes are created by the inward and outward facing E_{60} segments, the collective hydrophilic membrane thickness was estimated to be 40.8 nm. The entire vesicle membrane was determined by adding the thickness of the hydrophobic membrane to the hydrophilic membranes, resulting in a value of 40.8 + 3 = 43.8 nm. The Tf-DPEL vesicle diameter was approximately 160 nm, so the radius R_2 was set as 80 nm. The inner radius of R_1 was then calculated as 80 - 43.8 = 36.2 nm.

Since the accuracy of the numerical solution increases with the number of nodes, we divided the Tf-DPEL vesicle membrane into 101 nodes. The nodes of the vesicle membrane were uniformly spaced by a thickness h, where:

$$h = \frac{R_2 - R_1}{100} \tag{7}$$

Additionally, every vesicle membrane node was characterized by a drug concentration $C_{DOX,i}$, where i is an integer ranging from 1 to 101 that was used to index a specific node. Therefore, the first node at R_1 was assigned the DOX concentration $C_{DOX,1}$, and the second node positioned at $R_1 + h$ was assigned the DOX concentration $C_{DOX,2}$. This was repeated until node 101, which was positioned at $R_2 = R_1 + 100h$, with the DOX concentration $C_{DOX,101}$. A node was designated at the vesicle surface, which corresponded to a distance h away from the vesicle surface at R_2. This surface node was assigned the DOX concentration $C_{DOX,surface}$. Finally, the bulk solution beyond the vesicle surface was assigned the DOX concentration $C_{DOX,bulk}$.

Figure 1: A schematic of the Tf-DPEL vesicle when applying the method of lines. The vesicle bilayer was divided into 101 nodes from R_1 to R_2 with a thickness h between neighboring nodes. Each node was also characterized by its own DOX concentration, $C_{DOX,i}$. A node was also designated for the vesicle surface $C_{DOX,surface}$ where DOX undergoes convective mass transfer to the bulk solution, which has a concentration of $C_{DOX,bulk}$.

The non-boundary nodes, represented by $C_{DOX,i}$ for all i integer values excluding i=1 and $i = 101$, were each described by the PDE from Eq. (6):

$$\frac{\partial C_{DOX,i}}{\partial t} = D_{DOX}\left(\frac{\partial^2 C_{DOX,i}}{\partial r^2} + \frac{2}{r}\frac{\partial C_{DOX,i}}{\partial r}\right) for\ 2 \le i \le 100 \tag{8}$$

This resulted in 99 PDEs describing the change in concentration at each non-boundary node.

Additional equations were required to describe the nodes $C_{DOX,1}$, $C_{DOX,101}$, $C_{DOX,surface}$, and $C_{DOX,bulk}$ to complete the system of differential equations. Mole balances were used to obtain the boundary conditions. At R_1 and at any time *t*, moles of DOX from the aqueous core were lost as DOX diffused into the vesicle bilayer:

$$\frac{\partial\left(C_{DOX,core}\,V_1\right)}{\partial t} = D_{DOX}\,\frac{\partial C_{DOX,1}}{\partial r}\bigg|_{R_1} 4\pi {R_1}^2 \tag{9}$$

where $C_{DOX,core}$ is the DOX concentration in the Tf-DPEL vesicle aqueous core, and V_1 is the volume of the Tf-DPEL vesicle aqueous core, which was assumed to remain constant. At R_2 and at any time *t*, the moles of DOX leaving the vesicle membrane per time by diffusion was equal to the moles of DOX leaving the vesicle surface per time due to convective mass transfer to the bulk solution:

$$-D_{DOX}\,\frac{\partial C_{DOX,101}}{\partial r}\bigg|_{R_2} 4\pi {R_2}^2 = k_c\left(C_{DOX,surface} - C_{DOX,bulk}\right)4\pi(R_2+h)^2 \tag{10}$$

where k_c is the DOX mass transfer coefficient. Finally, a mass balance was used to describe $C_{DOX,bulk}$ where any gain in moles of drug in the bulk volume was due to mass transfer from the surface layer:

$$V_2\,\frac{dC_{DOX,bulk}}{dt} = k_c\left(C_{DOX,surface} - C_{DOX,bulk}\right)4\pi(R_2+h)^2 \tag{11}$$

where V_2 is the bulk volume set to 1000 mL to mimic the *in vitro* experiment.

Using the common assumption that equilibrium was immediately reached at the water-membrane boundaries, $C_{DOX,core}$ and $C_{DOX,surface}$ were related to the concentrations in the vesicle membrane across the interface by the partition coefficient K. The partition coefficient

was defined as the ratio of the DOX concentration in the vesicle membrane ($C_{DOX,mem}$) to the DOX concentration in an aqueous solution at equilibrium ($C_{DOX,aq}$):

$$K \equiv \frac{C_{DOX,mem}}{C_{DOX,aq}} = \frac{C_{DOX,1}}{C_{DOX,core}} = \frac{C_{DOX,101}}{C_{DOX,surface}} \tag{12}$$

Using Eq. (12), Eqs. (9) - (11) can therefore be simplified to the following equations, respectively:

$$\frac{\partial C_{DOX,1}}{\partial t} = \frac{KD_{DOX}}{V_1} \frac{\partial C_{DOX,1}}{\partial r}\bigg|_{R_1} 4\pi {R_1}^2 \tag{13}$$

$$-D_{DOX} \frac{dC_{DOX,101}}{dr}\bigg|_{R_2} 4\pi {R_2}^2 = k_c \left(\frac{C_{DOX,101}}{K} - C_{DOX,bulk} \right) 4\pi (R_2 + h)^2 \tag{14}$$

$$\frac{dC_{DOX,bulk}}{dt} = \frac{k_c \left(\frac{C_{DOX,101}}{K} - C_{DOX,bulk} \right) 4\pi (R_2 + h)^2}{V_2} \tag{15}$$

Finite difference equations and the method of lines were then used to transform the system of PDEs represented by Eqs. (8), (13), (14), and (15) into a system of ODEs by replacing the spatial derivatives, $\frac{\partial C_{DOX,i}}{\partial r}$ and $\frac{\partial^2 C_{DOX,i}}{\partial r^2}$, with finite differences. The first order and second order spatial derivatives of concentration were rewritten using the centered finite difference approach:

$$\frac{\partial C_{DOX,i}}{\partial r} = \frac{C_{DOX,i+1} - C_{DOX,i-1}}{h} \tag{16}$$

$$\frac{\partial^2 C_{DOX,i}}{\partial r^2} = \frac{C_{DOX,i+1} - 2C_{DOX,i} + C_{DOX,i-1}}{h^2} \tag{17}$$

The first order spatial derivative was also rewritten with either the forward finite difference:

$$\frac{\partial C_{DOX,i}}{\partial r} = \frac{C_{DOX,i+1} - C_{DOX,i}}{h} \tag{18}$$

or the backward finite difference:

$$\frac{\partial C_{DOX,i}}{\partial r} = \frac{C_{DOX,i} - C_{DOX,i-1}}{h} \tag{19}$$

303 depending on the location of the node being at the initial or final boundary position. These
304 algebraic expressions then replaced the spatial derivatives. When the centered finite differences
305 were applied to the non-boundary nodes described by Eq. (8), the PDEs became ODEs since
306 only one independent variable, t, remained as follows:

$$\frac{dC_{DOX,i}}{dt} = D_{DOX}\left(\frac{C_{DOX,i+1} - 2C_{DOX,i} + C_{DOX,i-1}}{h^2} + \frac{2}{r}\frac{C_{DOX,i+1} - C_{DOX,i-1}}{h}\right) \quad for\ 2 \le i \le 100 \tag{20}$$

307 The forward finite difference given by Eq. (18) was applied to Eq. (13) to yield:

$$\frac{dC_{DOX,1}}{dt} = \frac{KD_{DOX}}{V_1}\left(\frac{C_{DOX,2} - C_{DOX,1}}{h}\right)4\pi {R_1}^2 \tag{21}$$

308 The backward finite difference given by Eq. (19) was applied to Eq. (14) to obtain:

$$-D_{DOX}\left(\frac{C_{DOX,101} - C_{DOX,100}}{h}\right)4\pi {R_2}^2 = k_c\left(\frac{C_{DOX,101}}{K} - C_{DOX,bulk}\right)4\pi(R_2 + h)^2 \tag{22}$$

309 Solving for $C_{DOX,101}$ in Eq. (22) yields the following expression for $C_{DOX,101}$:

$$C_{DOX,101} = \frac{-\frac{k_c 4\pi(R_2 + h)^2}{D_{DOX}4\pi {R_2}^2}C_{DOX,bulk} + \frac{C_{DOX,100}}{h}}{\frac{1}{h} + \frac{k_c 4\pi(R_2 + h)^2}{D_{DOX}4\pi {R_2}^2 K}} \tag{23}$$

310 Equation (15), which described the change in moles in the bulk solution, was already an ODE
311 only dependent on time t. Therefore, Eqs. (15), (20), (21), and (23) were numerically solved to
312 predict concentration profiles and drug release.

Since the ODEs were differential equations with respect to time, initial conditions at each node were required to complete the solution. However, to accurately mimic the *in vitro* release study, the equations were solved twice: once to model drug release during the 24 h Tf conjugation period and a second time to predict the release profile during the *in vitro* release experiment following the conjugation. After DOX was encapsulated, Tf was conjugated to the vesicles to complete the targeted drug delivery system. However, the Tf conjugation lasted for 24 h, and the encapsulated DOX could be released during this time period. After the conjugation was complete, unconjugated Tf and the released DOX were removed, and the purified Tf-DPEL vesicles were used for the release study. Therefore, two sets of initial conditions were required as shown in Figure 2.

Figure 2: A schematic of the initial conditions used to solve the system of ODEs for the 24 h Tf-conjugation period and the release study. At the beginning of the Tf-conjugation, all of the drug was loaded within the vesicle core with a concentration C_0, and the DOX partitioned from the aqueous core to the vesicle membrane. After the 24 h period of Tf conjugation, some of the drug diffused across the vesicle bilayer and entered the bulk solution. After purification, the DOX in the bulk solution was removed, and the remaining concentration profile in the vesicle membrane became the initial conditions for modeling the release study.

Beginning with the Tf conjugation process, the DPEL vesicles were modeled to have DOX initially loaded homogeneously in V_1 at a concentration $C_{initial}$ (since $C_0\,(t_{conjugation}=0) = C_{initial}$) and not present anywhere else. Since we have been assuming that equilibrium is attained at the interface between the aqueous phase and the bilayer, the drug loaded in the core immediately partitioned to the first node. The initial condition at node 1 during the conjugation process was therefore given by:

$$C_{DOX,1}\left(t_{conjugation} = 0\right) = KC_{initial} \quad (24)$$

where $t_{conjugation}$ represents the time during the Tf conjugation process. Drug was initially loaded only in the aqueous core, so drug was not initially present anywhere else:

$$C_{DOX,i}\left(t_{conjugation} = 0\right) = 0 \; for \; i > 1 \quad (25)$$

$$C_{DOX,surface}\left(t_{conjugation} = 0\right) = 0 \quad (26)$$

$$C_{DOX,bulk}\left(t_{conjugation} = 0\right) = 0 \quad (27)$$

With these initial conditions, the system of ODEs was numerically integrated using the ode45 solver in MATLAB. The output from this solver was the DOX concentration at every node as a function of time, and the concentration profile was evaluated at $t = 24$ h.

Experimentally, the Tf-DPEL vesicles were purified after Tf conjugation to remove any unencapsulated DOX. Therefore, the bulk DOX concentration at the beginning of the release experiment was 0:

$$C_{DOX,bulk}\left(t_{release} = 0\right) = 0 \quad (28)$$

where $t_{release}$ represents the time point during the release study. Subsequently, the purified Tf-DPEL vesicles were placed within the dialysis bag for the release studies. Assuming that the Tf-DPEL vesicles placed in the dialysis bag had an identical DOX concentration profile as the Tf-DPELs after conjugation, the node concentrations at the end of the 24 h conjugation period became the initial conditions for modeling the release experiment, where:

$$C_{DOX,i}\left(t_{conjugation} = 24\right) = C_{DOX,i}\left(t_{release} = 0\right) \; for \; all \; i \quad (29)$$

The system of ODEs was numerically integrated again using the ode45 solver in MATLAB, which output the DOX concentration at every node as a function of time. Moles of drug released at any time t were therefore calculated as follows:

$$n_{release}\,(t_{release}) = C_{DOX,bulk}\,(t_{release})V_2 \tag{30}$$

We then needed to take a ratio of $n_{release}$ ($t_{release}$) to the initial number of moles in the vesicle. Since the moles of drug predicted to be released to the vesicle exterior during the conjugation process were negligible, the initial moles of drug in the vesicle at the beginning of the release study were estimated to be the same as the moles of drug that were in the vesicle at the beginning of the conjugation period. The initial moles of drug at the beginning of the release study were therefore calculated as follows:

$$n_{initial} = C_{initial}\,V_1 + \frac{4}{3}\pi\left[(R_1 + h)^3 - {R_1}^3\right]C_{initial}\,K \tag{31}$$

where $C_{initial}V_1$ corresponds to the initial moles of drug in the aqueous core at the beginning of the conjugation period, and $\frac{4}{3}\pi\left[(R_1 + h)^3 - {R_1}^3\right]C_{initial}\,K$ is equal to the initial moles of drug that immediately partitioned just inside the vesicle bilayer at the beginning of the conjugation period. The percent of drug released after $t_{release}$ hours was subsequently calculated as follows:

$$\%\ drug\ release(t_{release}) = \frac{n_{release}\,(t_{release})}{n_{initial}} \tag{32}$$

2.12. *In Vitro* Drug Release Experiment

To prepare for the *in vitro* release experiment, the Tf-DPEL vesicle sample was added to a dialysis bag (MWCO = 8,000 Da). The dialysis bag was then placed in a 1000 mL buffer containing 50 mM HEPES and 20 mM sodium bicarbonate. The release study was performed at 37°C. At selected time points, 20 µL of the Tf-DPEL vesicle suspension were removed from the

dialysis bag, and the DOX concentration was measured as previously discussed in Section 2.8. Time points were measured every 2 h for the first 8 h, and then at 24 h intervals until the end of the experiment at 192 h. Two bath exchanges were performed at 4 h and 24 h in order to maintain a low concentration of DOX in the exterior to promote mass transfer.

2.13. Cell Culture

The PC3 prostate cancer cell line was grown in RPMI 1640 media supplemented with 10% FBS and 1% P/S. These cells were maintained in a 37˚C humidified atmosphere with 5% CO_2 and passaged with standard cell culture protocols.

2.14. *In Vitro* Cytotoxicity Assay

One day prior to the cytotoxicity experiment, PC3 cells were seeded on a 96-well plate at a density of 7,500 cells/cm^2. After allowing the cells to grow overnight, the growth medium was aspirated. Tf-DPEL vesicles were added to RPMI 1640 medium with DOX concentrations varying from 0.01 to 3.16 μM. Subsequently, 100 μL of a suspension containing vesicles in the growth medium were added to each well. After a 96 h incubation period, the cell viability was determined with the MTS assay. Cell viability relative to the control (PC3 cells incubated in media without vesicles) was quantified by measuring the absorbance values at 490 and 700 nm. Cell growth inhibition was then compared against that of the non-targeted DPEL vesicles to evaluate the killing efficiency of the targeted vesicles.

3. Results and Discussion

3.1. Characterization of the Tf-DPEL Vesicles

The EL vesicles were polydisperse and in the micron size range after processing. By performing serial extrusion of the vesicles through 1000, 400, and 200 nm polycarbonate filters in the presence of a buffered ammonium sulfate solution, we were able to generate a

394 homogeneous population of vesicles with a diameter of 179 nm (Table 1). Since glutamate
395 residues were readily present on the surfaces of the EL vesicles, EDC/NHS chemistry was used
396 to conjugate mPEG and biPEG to the EL vesicles. PEG is a highly soluble polymer that provides
397 steric stability during the DOX loading process, and also has the potential in the future to provide
398 *in vivo* stability by preventing protein adsorption and aggregation (Ahl et al., 1997). The addition
399 of PEG to create PEGylated EL (PEL) vesicles slightly decreased the diameter to 173 nm. We
400 were not bothered by this decrease in size upon conjugation since the vesicles are supermolecular
401 structures generated by the noncovalent self-assembly of the polypeptides, and therefore,
402 changes in their packing properties within vesicles are possible. DOX was then encapsulated
403 within the vesicles using a modified pH-ammonium sulfate gradient to create the DPEL vesicles.
404 Finally, 10,000 Tf molecules per vesicle were added for conjugation to the biPEG linkers to
405 provide active targeting towards cancer cells and a method for cellular uptake of the vesicles. Tf
406 conjugation to create Tf-DPEL vesicles resulted in a diameter of 161 nm after purification with
407 size-exclusion chromatography. By simply controlling the initial size of the extruded EL
408 vesicles, we have been able to consistently obtain Tf-DPEL vesicles below 200 nm.
409

Table 1

Conjugation Step	Diameter (nm)	Polydispersity Index (PdI)	Loading Ratio
Extruded EL Vesicle	179 ± 4	0.170 ± 0.024	-
PEL Vesicle	173 ± 2	0.198 ± 0.006	-
Tf-DPEL Vesicle	161 ± 28	0.213 ± 0.027	15.3 ± 4.0

410

411 **Table 1:** The size and polydispersity index (PdI) of the vesicles as they were modified to create
412 the Tf-DPEL vesicles. The loading ratio could only be measured for the Tf-DPEL vesicles since
413 only the Tf-DPEL vesicles contained the DOX drug.
414

The diameter of the final Tf-DPEL vesicle construct satisfied the dual criteria for the size of a drug delivery vehicle. Firstly, the diameter was within the 60 to 400 nm range, indicating that it could take advantage of the enhanced permeability and retention (EPR) effect (Bae and Park, 2011). The EPR effect allows the nano-sized drug carriers to preferentially accumulate into tumor tissues due to the abnormal characteristics of the tumor tissue, which include increased vascular permeability and poor lymphatic drainage. The carrier can therefore reach high concentrations in the tumor compared to that in the plasma, thereby delivering the drugs preferentially to the cancer cells (Greish, 2010). Secondly, a Tf-DPEL vesicle diameter below 200 nm should enable the vesicles to be internalized via clathrin-mediated endocytosis (Rejman et al., 2004), (Choe et al., 2013), which is the pathway for the Tf ligand.

Vesicle stability was assessed using the polydispersity index (PdI). The PdI values of the EL, PEL, and Tf-DPEL vesicles were 0.170, 0.198, and 0.190, respectively (Table 1). All PdI values were within the range of 0 to 0.300, indicating a fairly homogeneous population (Badran et al., 2012) (Ibrahim et al., 2014). Despite undergoing multiple purification and conjugation steps, the vesicles maintained their overall integrity, possibly due to the intrinsic stability of polypeptide-based vehicles. The $E_{60}L_{20}$ block copolypeptides are larger building blocks than lipids, and therefore, experience greater van der Waals interactions to stabilize the vesicle structure. This allows for greater versatility for the EL vesicles as they can be modified after the self-assembly process, whereas liposomes often require PEG modification to the lipid prior to forming liposomes.

Vesicle stability was further evaluated by measuring the zeta potential throughout the conjugation process. A separate set of studies was performed in order to determine the zeta potential of the EL vesicles upon extrusion, PEGylation, and Tf conjugation. The values were

found to be -21.1 ± 2.3 mV for the extruded EL vesicles, -6.6 ± 3.5 mV upon PEGylation, and -19.5 ± 1.7 mV after conjugating Tf. Due to the no slip boundary condition being positioned further from the surface of charge, the decrease in the magnitude of the zeta potential was expected when the EL vesicles were coated with a layer of PEG. The zeta potential was also expected to become more negative with Tf conjugation as Tf is net negative at the pH of the buffer used during measurement. Similar to the PdI values, the resulting zeta potential values suggested that the vesicles remained stable after all conjugation procedures. Although -6.6 mV would generally represent instability, these vesicles were still stable due to the steric stabilization provided by the PEG.

In addition, we were interested in examining the morphology of the EL vesicles after PEGylation and Tf conjugation. Figure 3 shows a TEM image of the extruded EL vesicles after coating the surface with PEG and decorating the subsequent surface with Tf. The presence of unilamellar vesicles in Figure 3 suggests that the surface modifications provided by our conjugation protocol do not significantly alter or jeopardize the morphology of the original EL vesicles.

Figure 3: A transmission electron microscope (TEM) image of a uranyl acetate negatively stained EL vesicle suspension after PEGylation and Tf conjugation. Scale bar = 70 nm.

3.2. DOX Encapsulation Using a Modified pH-Ammonium Sulfate Gradient

DOX was successfully encapsulated within the Tf-DPEL vesicles using a modified pH-ammonium sulfate gradient method. First, a 0.5 M ammonium sulfate solution buffered to pH 5.5 was added to the EL vesicle suspension such that the encapsulated ammonium sulfate concentration was 0.05 M after serial extrusion. The exterior solution was buffered to pH 9.0

using Tris buffer to create the transmembrane pH-gradient so that DOX, originally present as doxorubicin hydrochloride, was deprotonated to its neutral form to more readily cross the hydrophobic bilayer of the vesicle to enter the core. Once inside the aqueous core, DOX could be protonated again due to the lower interior pH, preventing its diffusion back through the hydrophobic bilayer. Moreover, due to the presence of sulfate, a DOX-sulfate complex could form that is an insoluble gel-like solid fiber, further preventing diffusion back out of the vesicle. The DOX loading procedure was performed at 65°C for 1 h since previous reports state that increasing the incubation temperature above the phase transition temperature of a lipid bilayer increases the bilayer permeability to promote drug loading and improve the loading efficiency (Dos Santos et al., 2004). Using this modified transmembrane gradient, DOX was successfully encapsulated within the Tf-DPEL vesicles, achieving a loading ratio of 15.3.

3.3. Predicted and Measured *In Vitro* Drug Release Profiles for the Tf-DPEL Vesicles

To accurately predict DOX release from the Tf-DPEL vesicles, parameters such as the vesicle core radius R_1, the total radius R_2, the partition coefficient of DOX K, the diffusion coefficient of DOX in the vesicle bilayer D_{DOX}, and the convective mass transfer coefficient for DOX in water k_c were determined based on previously measured data or values reported in the literature.

R_1 and R_2 were determined as described in section 2.9. Mathematical Modeling of Drug Release. The DOX diffusion coefficient in the Tf-DPEL vesicle bilayer was selected based on values reported for a similar vesicle system. Eisenberg and coworkers investigated the release of DOX in polystyrene$_{310}$-*b*-poly(acrylic acid)$_{36}$ (PS$_{310}$-*b*-PAA$_{36}$) vesicles (Choucair et al., 2005). Since PS$_{310}$-*b*-PAA$_{36}$, which consists of a negatively-charged acrylic acid group and a neutral polystyrene group, self-assembles into vesicles, the EL vesicle bilayer was expected to have

similar properties to the PS_{310}-*b*-PAA_{36} vesicle bilayer. A D_{DOX} value of 2.5×10^{-17} cm^2/s was investigated for our model, which was in the range of values reported by the Eisenberg group for the diffusion coefficient of DOX in the PS_{310}-*b*-PAA_{36} vesicle polystyrene bilayer (Choucair et al., 2005).

To determine the value of the convective mass transfer coefficient for DOX in water, we first needed to estimate the Reynolds number, Re, given by:

$$Re = \frac{\rho v L}{\mu} \tag{33}$$

where ρ is the density of water, μ is the viscosity of water, L is the characteristic length, and v is the linear velocity of the fluid. However, since the *in vitro* release experiment was performed by stirring in a beaker, the linear velocity was replaced with $v = \omega r$, where ω is the angular velocity and r is the radial distance from the center of the beaker, to yield:

$$Re = \frac{\rho \omega r L}{\mu} \tag{34}$$

In addition to the density and viscosity of water, the characteristic length was estimated to be 160×10^{-9} m, which is the Tf-DPEL diameter. The angular velocity ω was measured to be 2.5 revolutions/sec according to the stir plate speed, and r was estimated to be 3 cm, half of the stir bar length. With these values, we calculated a Reynolds number of 0.0048. For this very low Reynolds number, the Nusselt number, Nu, is approximately equal to 2 based on the literature (Welty et al., 1984) and the Nusselt number is given by:

$$Nu = \frac{k_c L}{D_{DOX,water}} \tag{35}$$

where $D_{DOX,water}$ is the diffusivity of DOX in water. We estimated a $D_{DOX,water}$ value of 5×10^{-10} m^2/sec, which is a value similar to the diffusion coefficients of small molecules, such as sucrose

(Freitas Jr., 1999). From this, we calculated a DOX mass transfer coefficient k_c value of 0.00625 m/sec.

After compiling values for the parameters, the DOX concentration profile was numerically solved to model the release study, and the percent drug released was calculated at time points that corresponded to those in the *in vitro* experiment. Both the predicted and measured *in vitro* release profiles are plotted in Figure 4.

Figure 4: The measured and predicted *in vitro* release profiles are plotted over a time period of 192 h. The *in vitro* release data correspond to the triangles connected with the solid line, while the predicted release data are indicated by the squares connected with the dashed line.

The predicted release profile showed a faster release at the earlier time points with 55% of the drug being released by t=96 h. It then exhibited a fairly slow release until t=192 h where 64% of the drug was released. Similarly, for the experimentally measured release profile, a fast initial release was observed with 51.5% of the DOX being released after the first 24 h, and 63% of the DOX was released after 96 h. After the burst release, DOX was slowly released from t=24 h until t=192 h where 75.2% of the drug was released. This slow release at later time points has been observed with other vesicle systems, and it has been hypothesized as being due to the DOX-sulfate gel-like complexes in the aqueous core (Lasic et al., 1992). Specifically, DOX must first dissociate from the sulfate anion into solution in order to travel across the vesicle bilayer.

The main disparity between our predicted and measured release profiles is evident in the early stages of the release. The *in vitro* release profile exhibits a rapid burst effect within the first 24 h. This burst release was most likely due to drug being adsorbed on the outer surface of the vesicle bilayer. Since this drug was not encapsulated within the vesicle, it was immediately released when the release study was performed. Since our mathematical model did not consider desorption of drug from the vesicle surface, our predicted release profile did not exhibit the same

level of burst release. Nevertheless, our mathematical model was able to reasonably predict the *in vitro* release profile with no fitted parameters. Additionally, the mathematical model has given us insight into the parameters that can be varied in order to modify future release profiles, such as the type of drug that is encapsulated and the dimensions of the drug delivery carrier.

3.4. Drug Delivery Efficacy of the Tf-DPEL Vesicle

To mimic the *in vivo* conditions of Tf receptor (TfR) overexpression on cancer cells, the PC3 human prostate cancer cell line was used for the cytotoxicity studies. PC3 cells exhibit TfR levels comparable to their *in vivo* expression, which are 10-fold greater than that of human benign prostatic hyperplasia specimens (Keer et al., 1990). The Tf-DPEL vesicles and their non-targeted counterpart, the DPEL vesicles, were administered to the PC3 prostate cancer cells over a range of concentrations for 96 h. Cell viability was determined using the MTS assay.

The results of the cytotoxicity assay demonstrate that, for every percent of cellular growth inhibition, a lower drug concentration was required for the Tf-DPEL vesicles than the DPEL vesicles to achieve the same percent inhibition (Figure 5). The IC_{50} value, which is the concentration of drug required to achieve 50% cell inhibition, of the Tf-DPEL and DPEL vesicles were 0.087 and 0.133 μM, respectively, corresponding to a 1.53-fold difference. Since the presence of Tf was the only variation between the Tf-DPEL and the DPEL vesicles, the increase in growth inhibition was most likely due to the targeting characteristics of Tf. Specifically, upon entering the cell via receptor-mediated endocytosis, the Tf-DPEL vesicles were able to release the encapsulated DOX directly within the cell, and this released DOX could subsequently enter the nucleus and exert its cytotoxic effects. This suggests that the addition of Tf to the DPEL vesicles successfully improved the drug delivery efficacy as hypothesized.

Figure 5: *In vitro* cytotoxicity results for the DPEL and Tf-DPEL vesicles in PC3 cells. The Tf-DPEL vesicle data correspond to the triangles connected with the solid line, while the DPEL vesicle data are indicated by the squares connected with the dashed line. The IC_{50} value of the DPEL was 0.133 μM, and the IC_{50} value of the Tf-DPEL was 0.087 μM.

5. Conclusions

This study represents the first investigation of the drug delivery properties of the EL vesicles. We successfully developed a stable, targeted drug delivery system by encapsulating DOX within PEGylated EL vesicles using a modified pH-ammonium sulfate gradient method and conjugated Tf to the vesicles to provide active targeting. The resulting Tf-DPEL vesicles were within the size range that could take advantage of both passive and active targeting. Subsequently, we derived a mathematical model to predict drug release from the Tf-DPEL vesicles. The mathematical model captured the diffusion of DOX across the vesicle bilayer and convective mass transfer to the bulk solution. Additionally, drug release during the 24 h Tf-conjugation period was considered in the model in order to accurately represent the *in vitro* release study protocols. The system of differential equations was solved numerically using the method of lines to yield a predicated release profile that compared favorably with our measured profile with no fitted parameters. We believe that this mathematical model can be used in the future to estimate the effects of adjusting certain parameters on drug release, which is an important feature for drug carriers. Finally, our *in vitro* cytotoxicity studies demonstrated that the Tf-DPEL vesicles showed an improved drug delivery efficacy with a 1.53 fold decrease in the IC_{50} value due to the increase in uptake of the vesicles with the addition of the targeting ligand. The theoretical and experimental studies reported here demonstrate the potential for using EL vesicles in the clinical setting.

Acknowledgments

This work was supported by the National Science Foundation DMR 1308081. The authors acknowledge the help of Wong Hoi Hui and the use of instruments at the Electron Imaging Center for NanoMachines supported by NIH (1S10RR23057 to ZHZ) and CNSI at UCLA.

References

Ahl, P.L., Bhatia, S.K., Meers, P., Roberts, P., Stevens, R., Dause, R., Perkins, W.R., Janoff, A.S., 1997. Enhancement of the in vivo circulation lifetime of l-α-distearoylphosphatidylcholine liposomes: importance of liposomal aggregation versus complement opsonization. Biochimica et Biophysica Acta 1329, 370-382.

Aisen, P., Listowsky, I., 1980. Iron transport and storage proteins. Annu Rev Biochem 49, 357-393.

Badran, M., Shalaby, K., Al-Omrani, A., 2012. Influence of the flexible liposomes on the skin deposition of a hydrophilic model drug, carboxyfluorescein: dependency on their composition. ScientificWorldJournal 2012, 134876.

Bae, Y.H., Park, K., 2011. Targeted drug delivery to tumors: Myths, reality and possibility. Journal of Controlled Release 153, 198-205.

Carlsen, A., Lecommandoux, S., 2009. Self-assembly of polypeptide-based block copolymer amphiphiles. Current Opinion in Colloid & Interface Science 14, 329-339.

Choe, U.J., Rodriguez, A.R., Lee, B.S., Knowles, S.M., Wu, A.M., Deming, T.J., Kamei, D.T., 2013. Endocytosis and Intracellular Trafficking Properties of Transferrin-Conjugated Block Copolypeptide Vesicles. Biomacromolecules 14, 1458-1464.

Choucair, A., Soo, P.L., Eisenberg, A., 2005. Active Loading and Tunable Release of Doxorubicin from Block Copolymer Vesicles. Langmuir 21, 9308-9313.

Deming, T.J., 1997. Facile synthesis of block copolypeptides of defined architecture. Nature 390, 386-389.

Dos Santos, N., Cox, K.A., McKenzie, C.A., van Baarda, F., Gallagher, R.C., Karlsson, G., Edwards, K., Mayer, L.D., Allen, C., Bally, M.B., 2004. pH gradient loading of anthracyclines into cholesterol-free liposomes: enhancing drug loading rates through use of ethanol. Biochim Biophys Acta 1661, 47-60.

Freitas Jr., R.A., 1999. Nanomedicine, Volume I: Basic Capabilities. Landes Bioscience, Georgetown.

Greish, K., 2010. Enhanced Permeability and Retention (EPR) Effect for Anticancer Nanomedicine Drug Targeting. Cancer Nanotechnology, Methods in Molecular Biology 624, 25-37.

Holowka, E.P., Pochan, D.J., Deming, T.J., 2005. Charged polypeptide vesicles with controllable diameter. J Am Chem Soc 127, 12423-12428.

Ibrahim, W.M., AlOmrani, A.H., Yassin, A.E., 2014. Novel sulpiride-loaded solid lipid nanoparticles with enhanced intestinal permeability. International journal of nanomedicine 9, 129-144.

Imordino, M.L., Dosio, F., Cattel, L., 2006. Stealth liposomes: review of the basic science, rationale, and clinical applications, existing and potential. Int J Nanomedicine 1, 297-315.

617 Karin, M., Mintz, B., 1981. Receptor-mediated endocytosis of transferrin in developmentally
618 totipotent mouse teratocarcinoma stem cells. Journal of Biological Chemistry 256, 3245-
619 3252.
620 Keer, H.N., Kozlowski, J.M., Tsai, Y.C., Lee, C., McEwan, R.N., Grayhack, J.T., 1990. Elevated
621 transferrin receptor content in human prostate cancer cell lines assessed in vitro and in
622 vivo. J Urol. 143, 381-385.
623 Keizer, H.G., Pinedo, H.M., Schuurhuis, G.J., Joenje, H., 1990. Doxorubicin (adriamycin): A
624 critical review of free radical-dependent mechanisms of cytotoxicity. Pharmacology &
625 Therapeutics 47, 219-231.
626 Lasic, D.D., Frederik, P.M., Stuart, M.A., Barenholz, Y., McIntosh, T.J., 1992. Gelation of
627 liposome interior: A novel method for drug encapsulation. FEBS 312, 255-258.
628 Mayle, K.M., Le, A.M., Kamei, D.T., 2012. The Intracellular Trafficking Pathway of
629 Transferrin. Biochim Biophys Acta 1820, 264–281.
630 Rejman, J., Oberle, V., Zuhorn, I.S., Hoekstra, D., 2004. Size-dependent internalization of
631 particles via the pathways of clathrin- and caveolae-mediated endocytosis. The Biochemical
632 Journal 377, 156-169.
633 Sahoo, S.K., Jain, T.K., Reddy, M.K., Labhasetwar, V., 2008. Nano-Sized Carriers for Drug
634 Delivery. Humana Press.
635 Tacar, O., Sriamornsak, P., Dass, C.R., 2012. Doxorubicin: an update on anticancer molecular
636 action, toxicity and novel drug delivery systems. Journal of Pharmacy and Pharmacology
637 65, 157-170.
638 Welty, J.R., Wicks, C.E., Wilson, R.E., 1984. Fundamentals of momentum, heat, and mass
639 transfer, 3rd ed. Wiley, New York.

640

641

Figure 1

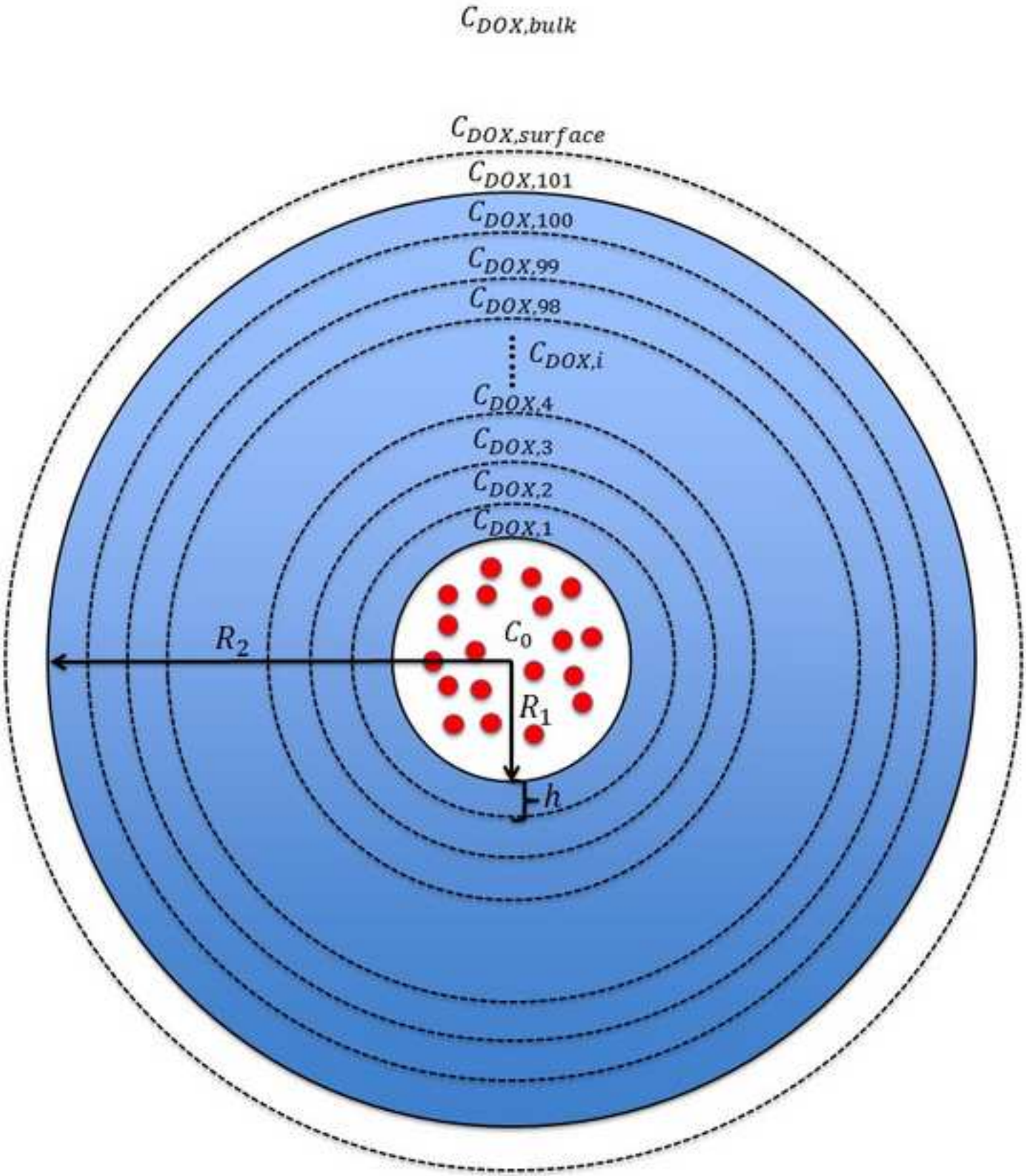
$C_{DOX,bulk}$
$C_{DOX,surface}$
$C_{DOX,101}$
$C_{DOX,100}$
$C_{DOX,99}$
$C_{DOX,98}$
$C_{DOX,i}$
$C_{DOX,4}$
$C_{DOX,3}$
$C_{DOX,2}$
$C_{DOX,1}$
C_0
R_2
R_1
h

Figure 2

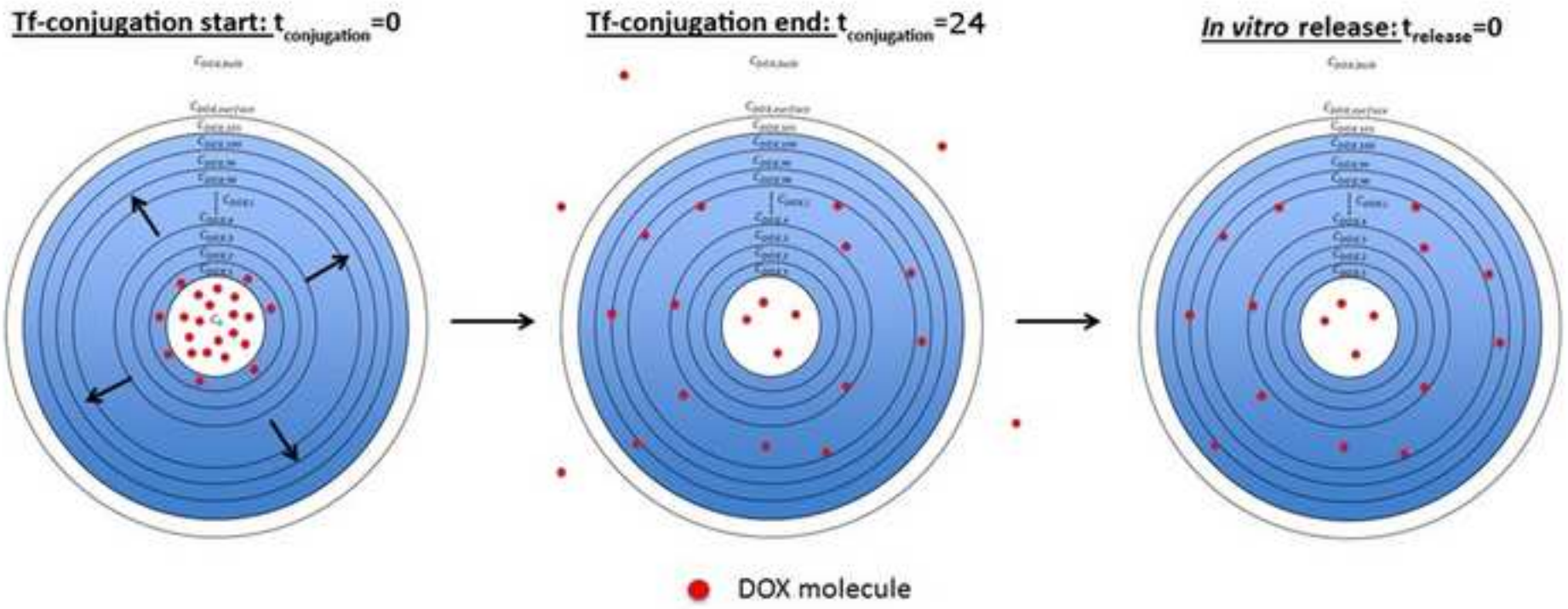
Tf-conjugation start: t conjugation =0
Tf-conjugation end: t conjugation =24
In vitro release: t release =0
DOX molecule

Figure 3

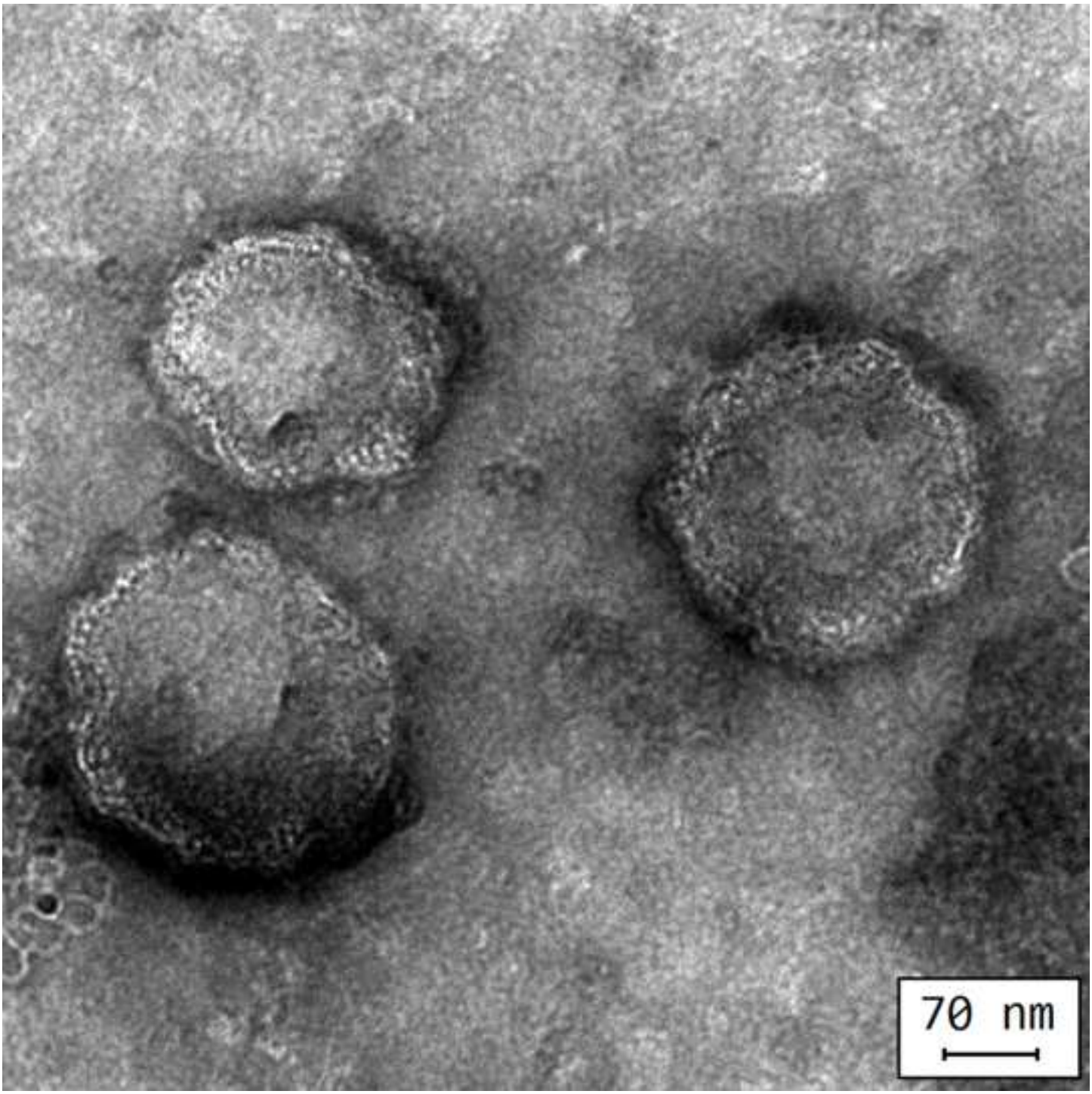

Figure 4

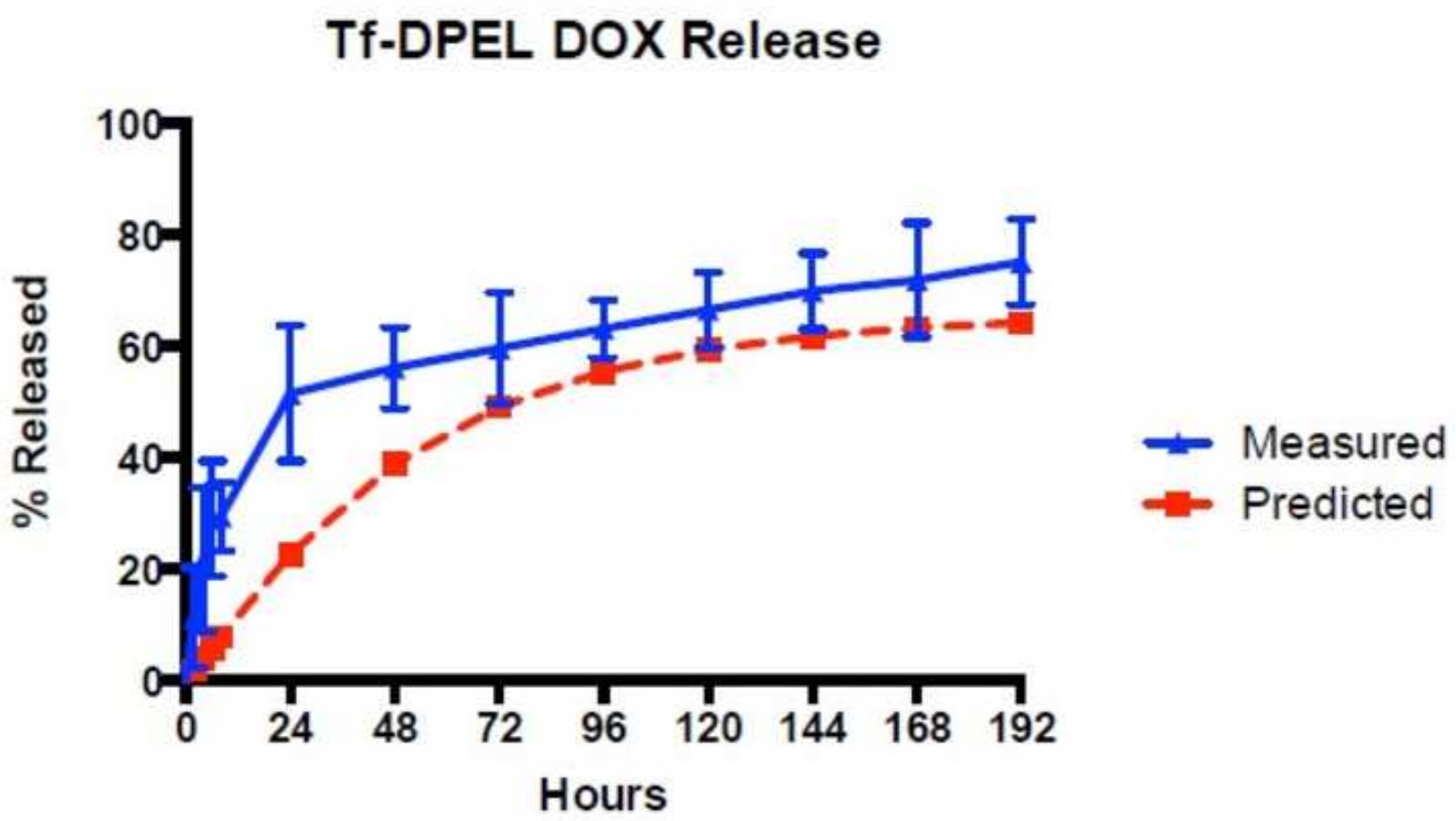
Tf-DPEL DOX Release
% Released
100
80
60
40
20
0
0
24
48
72
96
120
144
168
192
Hours
Measured
Predicted

Figure 5

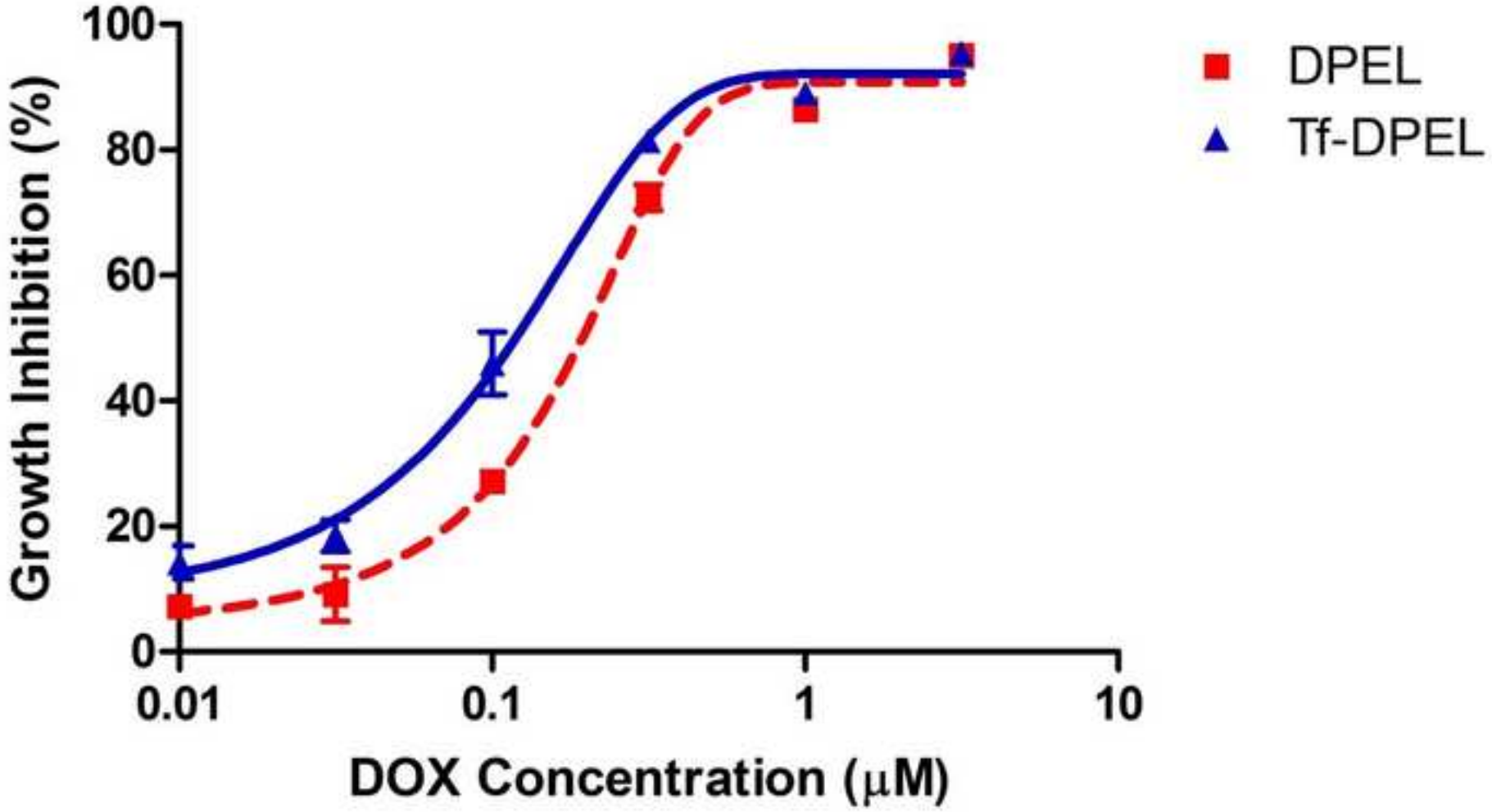
Growth Inhibition (%)
100
80
60
40
20
0
0.01
0.1
1
10
DOX Concentration (μM)
DPEL
Tf-DPEL